ISTANBUL TECHNICAL UNIVERSITY ★ GRADUATE SCHOOL

EXPERIMENTAL STUDY ON DISCRETE VORTEX GUST ENCOUNTERED BY A FLAT PLATE AT 45° WING SWEEP

M.Sc. THESIS

Ozan İBRAHİMAĞAOĞLU

Department of Aeronautics and Astronautics Engineering

Aeronautics and Astronautics Engineering Programme

AUGUST 2025

ISTANBUL TECHNICAL UNIVERSITY ★ GRADUATE SCHOOL

EXPERIMENTAL STUDY ON DISCRETE VORTEX GUST ENCOUNTERED BY A FLAT PLATE AT 45° WING SWEEP

M.Sc. THESIS

Ozan İBRAHİMAĞAOĞLU
(511221209)

Department of Aeronautics and Astronautics Engineering

Aeronautics and Astronautics Engineering Programme

Thesis Advisor: Prof. Dr. Nuriye Leman Okşan ÇETİNER YILDIRIM

AUGUST 2025

ISTANBUL TEKNİK ÜNİVERSİTESİ ★ LİSANSÜSTÜ EĞİTİM ENSTİTÜSÜ

45° OK AÇILI DÜZ PLAKA KANADIN GİRDAP TÜRÜ TEKİL SAĞANAK KARŞILAŞMASININ DENEYSEL İNCELENMESİ

YÜKSEK LİSANS TEZİ

Ozan İBRAHİMAĞAOĞLU
(511221209)

Uçak ve Uzay Mühendisliği Anabilim Dalı

Uçak ve Uzay Mühendisliği Programı

Tez Danışmanı: Prof. Dr. Nuriye Leman Okşan ÇETİNER YILDIRIM

AĞUSTOS 2025

Ozan İbrahimağaoğlu, a M.Sc. student of ITU Graduate School student ID 511221209, successfully defended the thesis entitled "EXPERIMENTAL STUDY ON DISCRETE VORTEX GUST ENCOUNTERED BY A FLAT PLATE AT 45˚ WING SWEEP", which he prepared after fulfilling the requirements specified in the associated legislations, before the jury whose signatures are below.

Thesis Advisor : **Prof. Dr. Okşan ÇETİNER YILDIRIM** ....
Istanbul Technical University

Jury Members : **Prof. Dr. Fırat Oğuz EDİS** ....
Istanbul Technical University

Asst. Prof. Dr. Onur SON ....
Gebze Technical University

Date of Submission : 5 August 2025
Date of Defense : 20 August 2025

To my family,

FOREWORD

I would like to express my deepest gratitude to my supervisor, Prof. Dr. N. L. Okşan Çetiner Yıldırım, whose guidance has shaped my journey throughout my master's studies. From the very beginning, she has instilled in me the values of academic integrity, perseverance, and the mindset of a good researcher. Her vast knowledge, unwavering support, and genuine interest in my work have been invaluable. Moreover, her encouragement played a decisive role in my decision to pursue an academic career, and for that, I am sincerely thankful.

I am equally indebted to Öğr. Gör. Murat Sarıtaş for his continuous assistance during my experiments, post-processing stages, and at every challenging turn of this study. His willingness to share his expertise, provide direction, and offer help whenever needed has greatly contributed to the completion of this research. I would also like to thank my lab partner and dear friend Kübra Soy, who was there when I took my very first steps in experimental work. At a time when I had no prior experience in the field, she generously shared her knowledge and helped me grow in both skill and confidence.

A special acknowledgment is due to my esteemed teacher, Asst. Prof. Dr. Hayri Acar, who has been far more than an academic mentor to me. Since the very first day of my undergraduate studies, he has stood by me as a constant source of wisdom, encouragement, and moral guidance. His presence has illuminated my path, sometimes with an advice, sometimes with a quiet support, and always with genuine care. He is, and will always remain, one of the finest examples of how to be not only a great lecturer but also a truly good person. I carry an enduring sense of gratitude and respect for everything he has given to me.

Also, my heartfelt gratitude goes as well to my lifelong friends Benan Tüllüoğlu, Cem Değimli, and Başak Acarlar, who have been by my side through every high and low, offering their love, encouragement, and friendship over the years. Moreover, I would like to extend my thanks to my colleagues and friends Tunahan Günay, Oğuz Özdoğan, and Orhan Hızalan for their steadfast support and companionship.

Lastly, and most importantly, I owe everything to my family; my mother, father, and my dearest sister. They are my home, my foundation, and my greatest source of strength. From my earliest memories to this very moment, they have been the unwavering presence behind every step I have taken, lifting me in moments of doubt and celebrating with me in moments of joy. Their sacrifices, love, and belief in me are beyond anything I could ever repay, and my achievements are as much theirs as they are mine. No words could truly encompass the depth of my gratitude, but it is with all my heart that I dedicate this work to them.

August 2025 Ozan İBRAHİMAĞAOĞLU

TABLE OF CONTENTS

Page

ABBREVIATIONS

DPIV	**:** Digital Particle Image Velocimetry
CFD	**:** Computational Fluid Dynamics
MAV	**:** Micro Aerial Vehicles
UAV	**:** Unmanned Aerial Vehicles
AR	**:** Aspect Ratio
GR	**:** Gust Ratio
LEV	**:** Leading-edge Vortex
PSP	**:** Polyamid Seeding Particles

SYMBOLS

Δx	: Horizontal distance between gust generator and wing model
Δy	: Vertical distance between gust generator and wing model
h	: Vortex trajectory height
T	: Half-rotation duration of the gust generator
c	: Wing chord length
s	: Wingspan
η	: Non-dimensional spanwise location
t*	: Convective time
U_∞	: Freestream velocity
C_L	: Lift coefficient
V_p	: Propagation speed

LIST OF TABLES

Page

LIST OF FIGURES

EXPERIMENTAL STUDY ON DISCRETE VORTEX GUST ENCOUNTERED BY A FLAT PLATE AT 45° WING SWEEP

SUMMARY

Aircraft operating in atmospheric environments are routinely subjected to unsteady aerodynamic disturbances caused by gusts, vortices, and turbulent flow structures. These disturbances can severely affect flight stability, maneuverability, and structural integrity, particularly for small-scale and low-inertia aerial vehicles such as Micro Air Vehicles (MAVs) and Unmanned Aerial Vehicles (UAVs).

Despite the importance of gust response, the vast majority of existing research has concentrated on two-dimensional wings. While a considerable body of work exists on gust response for flat plates at no wing sweep, studies incorporating with wing sweep, especially at moderate to high sweep angles, are still rare. The influence of wing sweep introduces additional complexities such as spanwise flow development, asymmetric vortex breakdown at high sweep angles, and directional sensitivity to the incoming gust, which cannot be captured by purely two-dimensional models. Given the increasing demand for agile and gust-resilient aerial platforms, there is a strong need to experimentally study these interactions under controlled laboratory conditions.

The primary objective of this study is to experimentally investigate the aerodynamic response of a flat plate wing model with a 45° sweep angle when subjected to discrete vortex gusts. The scope of this work encompasses both quantitative flow visualization and aerodynamic force assessment, enabling a unified view of the fluid-structure interaction under unsteady gust environments. The results are expected to clarify the influence of sweep geometry, symmetry plane mirror effect, and tip geometry, thereby contributing to gust modeling strategies for swept-wing designs.

To explore the unsteady aerodynamic response under controlled gust conditions, a series of water channel experiments are conducted using a gust generation mechanism. The gusts are generated via controlled rotational motion of a flat-plate gust generator, simulate localized, transient disturbances that resemble vortex gust phenomena encountered in real-world scenarios. By varying key parameters such as the vertical distance between the gust generator and the wing (Δy) and the half-rotation duration of the generator (T), the study aims to systematically characterize how the gust encounter, trajectory, and the sweep angle affect the resulting force dynamics and flow structures. Three distinct wing configurations are examined: a no-swept flat plate, a 45° swept flat plate, and a 45° swept plate with a sharp tip modification. For each configuration, multiple test cases are executed across two vortex trajectories (h/c), which are adjusted by varying Δy, and three half-rotation durations (T), resulting in a comprehensive matrix of 6 cases. High-resolution force measurements and Digital Particle Image Velocimetry (DPIV) analyses are conducted to quantify vorticity fields in conjuction with lift coefficients. Reynolds number of 10,000 is maintained throughout all experiments. This experimental setup enables both high temporal resolution of aerodynamic loads and direct visualization of vortex-wing interaction

mechanisms, forming a strong foundation for interpreting the complex, transient flow phenomena associated with discrete gust encounters.

In this study, discrete vortex gust encounter experiments are conducted on several wing configurations, including a no-swept flat plate wing and two swept wing models with differing tip geometries: a sharp tip and a tip aligned with the freestream. Additionally, two submergence levels are tested for the swept wing models to examine their effect on gust response. Comparison between standard submergence level, where the water level coincides with the wing's symmetry axis (root section), and a deeper submergence including 15% of the opposite half-span (creating a partially V-shaped model), revealed no significant influence on the aerodynamic response. Similarly, the tip geometry difference demonstrated negligible differences in aerodynamic response.

While the variations in submergence level and tip geometry showed minimal impact under the specific test conditions, the influence of sweep angle emerged as a critical factor. The sweep angle introduced a notable time delay in the lift response to vortex gust encounters and a reduction of lift amplitude compared to the no-swept configuration. Additionally, a time shift in lift response observed along the wing span indicates that different sections of the swept wing experienced the gust at slightly different times. This phase lag was confirmed by comparing instantaneous flow visualizations along the span. These observations support the value of simplified modeling techniques, such as time-shifted lift profiles, to approximate complex gust interactions on swept configurations.

45° OK AÇILI DÜZ PLAKA KANADIN GİRDAP TÜRÜ TEKİL SAĞANAK KARŞILAŞMASININ DENEYSEL İNCELENMESİ

ÖZET

Atmosferik ortamlarda faaliyet gösteren hava araçları, genellikle sağanaklar, girdaplar ve türbülanslı akış yapılarından kaynaklanan kararsız aerodinamik bozunumlara maruz kalmaktadır. Bu bozunumlar, özellikle Mikro Hava Araçları (MAV'ler) ve İnsansız Hava Araçları (İHA'lar) gibi küçük ölçekli ve düşük ataletli hava araçları için uçuş kararlılığı, manevra kabiliyeti ve yapısal bütünlük üzerinde ciddi etkiler yaratabilir. Daha büyük ticari uçaklar bu tür bozunumları yüksek ataletleri ve gelişmiş uçuş kontrol sistemleri sayesinde tolere edebilirken, daha küçük hava araçları orta şiddetteki sağanak karşılaşmalarına karşı bile oldukça savunmasızdır. Bu durum sağanak tepkisinin analizini aerodinamik araştırmaların kritik bir alanı haline getirmektedir. Özellikle şehir içi bölgelerde, gemi üst yapılarının arkasında veya arazi düzensizliklerinin yakınında karşılaşılan girdap sağanaklarının hava aracıyla nasıl etkileşime girdiğini anlamak özel bir zorluk teşkil etmektedir. Sürekli sağanaklardan farklı olarak, tekil girdap sağanakları özellikle ok açılı kanatlar veya karmaşık geometrilerle etkileşime girdiklerinde, taşıma kuvveti, sürükleme kuvveti ve yunuslama momenti gibi değerlerde ani değişimlere ve akış ayrılmasına neden olabilecek oldukça kararsız, doğrusal olmayan tepkiler oluşturabilirler.

Sağanak karşılaşmalarının önemi göz önüne alındığında, mevcut araştırmaların büyük çoğunluğu iki boyutlu kanatlar üzerinde yoğunlaşmıştır. Ok açılı olmayan düz plakalar için sağanak tepkisine dair önemli miktarda çalışma mevcut olsa da, kanat ok açısını da içeren çalışmalar, özellikle orta ve yüksek ok açıları için, halen oldukça nadirdir. Kanadın ok açılı olması, kanat açıklığı boyunca akış gelişimi, yüksek ok açılarında asimetrik girdap ayrılması ve gelen sağanağa yönsel hassasiyet gibi yalnızca iki boyutlu modellerle yakalanamayan ek karmaşıklıklar getirmektedir. Giderek daha çevik ve sağanaklara dayanıklı hava araçlarına olan talep göz önüne alındığında, bu etkileşimlerin kontrollü laboratuvar ortamlarında deneysel olarak incelenmesi büyük bir gerekliliktir. Bu, özellikle sağlam kontrol stratejileri, uyarlanabilir hava aracı gövde konfigürasyonları ve gerçek zamanlı sağanak önleme sistemlerinin tasarımına yönelik kritik bilgiler sağlar. Yüksek ok açılarına sahip düz plakaların ayrık girdap sağanaklarına verdiği tepkilerin anlaşılması, mevcut aerodinamik literatürdeki önemli bir boşluğu doldurmakta ve sağanak bakımından zengin ortamlarda faaliyet gösteren yeni nesil hava araçları için değerli bilgiler sunmaktadır.

Bu çalışmanın temel amacı, 45° ok açısına sahip düz plaka kanat modelinin girdap türü tekil sağanaklara maruz kaldığında gösterdiği aerodinamik tepkiyi deneysel olarak araştırmaktır. Bu kapsamda, hem akım görüntüleme hem de aerodinamik kuvvet ölçümleri gerçekleştirilmiş, böylece kararsız sağanak ortamlarındaki sağanak-kanat etkileşimi bütüncül bir bakış açısıyla incelenmiştir. Elde edilen sonuçların, ok açılı kanat geometrisi, simetri düzlemi ayna etkisi ve kanat uç geometrisinin etkilerini

açıklığa kavuşturması ve ok açılı kanat tasarımları için sağanak modelleme stratejilerine katkı sağlaması beklenmektedir.

Kontrollü sağanak koşulları altında kararsız aerodinamik tepkileri incelemek amacıyla, serbest su yüzeyine sahip bir su kanalında, bir sağanak üretim mekanizması kullanılarak bir dizi deney gerçekleştirilmiştir. Sağanaklar, dikdörtgensel bir düz plakanın (sağanak üreteci) saat yönünde kontrollü yarım tur dönme hareketi yoluyla oluşturulmuş ve gerçek dünyadaki girdap türü sağanak olgularına benzeyen lokal, geçici bozunumları taklit etmiştir. Sağanak üreteci ile kanat modeli arasındaki düşey mesafe (Δy) ve sağanak üreteci düz plakanın yarı tur dönüş süresi (T) gibi temel parametreler değiştirilerek, sağanak karşılaşmasının, girdabın izlediği yörüngenin ve ok açısının aerodinamik kuvvetler ve akış yapıları üzerindeki etkileri sistematik olarak karakterize edilmeye çalışılmıştır. Bu çalışmada, ok açısız düz plaka, 45° ok açılı düz plaka ve keskin uç modifikasyonuna sahip 45° ok açılı düz plaka olmak üzere üç adet kanat modeli kullanılarak çeşitli kanat konfigürasyonları üzerinde girdap türü tekil sağanak karşılaşması deneyleri gerçekleştirilmiştir. Ek olarak, ok açılı kanat modelleri için iki farklı su seviyesi (su seviyesi kanat simetri ekseniyle çakışacak şekilde ve su seviyesi kanat simetri eksenin öteki tarafına yükseltilerek yarı kanat açıklığının %15'lik kısmını da dahil edecek şekilde) test edilerek bu parametrenin sağanak tepkisi üzerindeki etkisi araştırılmıştır. Her bir kanat modeli için, iki farklı girdap yörüngesine ($h/c = 0, -0.75$) karşılık gelen Δy değerleri ve üç farklı yarı dönüş süresi (T = 3s, 4s, 6s) kullanılarak altı deney senaryosu içeren kapsamlı bir matris oluşturulmuştur. Tüm deneylerde, hücum açısı sıfır derece olarak ve Reynolds sayısı 10,000 olarak sabit tutulmuştur.

Aerodinamik katsayıları belirlemek amacıyla yüksek çözünürlüklü kuvvet ölçümleri yapılmıştır. Zamana bağlı bu kuvvet ve moment ölçümleri için altı bileşenli bir Kuvvet/Tork sensörü kullanılmaktadır. Sensör, kanat modelinin bağlantı çubuğu ile servo motora bağlı dikey çubuk arasına yerleştirilmiştir. Bağlantı çubuğu, kanat kök kesitinin hücum kenarından geçerek kanat açıklığı (z ekseni) yönünde hizalanmayı sağlamaktadır.

Kuvvet ölçümlerinin yanı sıra akış yapıları ve girdap alanlarını elde etmek için Dijital Parçacık Görüntüleme Hızölçer (DPIV) ölçüm tekniği uygulanmıştır. Ok açılı kanat durumunda üç boyutlu etkileri anlamak için, her bir kanat konfigürasyonunda kanat açıklığı boyunca üç ayrı kesitte (η = 0.25, 0.5, 0.825) akım görüntüleme ölçümleri yapılmıştır.

Akım görüntüleme ve kuvvet ölçümleri eş zamanlı olarak yapılmış olup, bu deney düzeneği, aerodinamik yüklerin yüksek zamansal çözünürlükte ölçülmesini ve girdap-kanat etkileşim mekanizmalarının doğrudan görselleştirilmesini mümkün kılmış, tekil sağanak karşılaşmalarına özgü karmaşık ve geçici akış olgularının yorumlanması için güçlü bir temel oluşturmuştur.

Elde edilen sonuçlar ışığında, su seviyesinin kanat simetri ekseni (kök kesiti) ile çakıştığı standart seviyedeki konfigürasyon ile kanadın karşı tarafındaki yarı açıklığın %15'lik kısmını da kapsayacak şekilde daha derin bir su seviyesinin (kısmen V-şekilli bir model oluşturarak) karşılaştırılması, aerodinamik tepki üzerinde belirgin bir etkisinin olmadığını göstermiştir. Benzer şekilde, uç geometrisindeki farklılık da karşılaştırılmış ve bu farklılık aerodinamik tepki açısından ihmal edilebilir düzeyde fark yaratmıştır.

Su seviyesi ve kanat uç geometrisindeki değişikliklerin belirtlilen deney koşulları altında neredeyse hiç etki göstermediği gözlemlenirken, kanat ok açısının etkisi kritik bir faktör olarak öne çıkmıştır. Ok açısı, girdap türü sağanak karşılaşmasına verilen taşıma tepkisinde dikkate değer bir zaman gecikmesi ve ok açısız kanat konfigürasyonuna kıyasla taşıma katsayısı genliğinde bir azalma yaratmıştır. Ayrıca, kanadın sağanak tarafından indüklenmiş taşıma katsayısında gözlemlenen bu zaman kayması, ok açılı kanadın kanat açıklığı boyunca farklı kesitlerinin sağanakla daha farklı zamanlarda karşılaştığını göstermektedir. Bu faz gecikmesi, kanat açıklığı boyunca farklı kesitlerde yapılan akım görüntüleme deneylerinden elde edilen anlık akım görselleştirmeleriyle de doğrulanmıştır. Bu gözlemler, taşıma katsayısı verisinin kanat kesidi bazlı zamanda kaydırılması gibi basitleştirilmiş modelleme tekniklerinin, ok açısı verilmiş kanat konfigürasyonlarının karmaşık sağanaklarla etkileşimlerini yaklaşık olarak elde etmede değerli olabileceğini göstermektedir.

1. INTRODUCTION

Aircraft operating in atmospheric environments are routinely subjected to unsteady aerodynamic disturbances caused by gusts, vortices, and turbulent flow structures. These disturbances can severely affect flight stability, maneuverability, and structural integrity, particularly for small-scale and low-inertia aerial vehicles such as Micro Air Vehicles (MAVs) and Unmanned Aerial Vehicles (UAVs). While larger commercial aircraft can absorb such disturbances due to their high inertia and robust flight control systems, smaller aerial vehicles are significantly more vulnerable to even moderate gust encounters, making gust response analysis a critical area of aerodynamic research [1].

Despite the importance of gust response, the vast majority of existing research has concentrated on two-dimensional wings. While a considerable body of work exists on gust response for flat plates at no wing sweep, studies incorporating with wing sweep, especially at moderate to high sweep angles, are still rare. The influence of wing sweep introduces additional complexities such as spanwise flow development, asymmetric vortex breakdown at high sweep angles, and directional sensitivity to the incoming gust, which cannot be captured by purely two-dimensional models [1-3].

Given the increasing demand for agile and gust-resilient aerial platforms, there is a strong need to experimentally study these interactions under controlled laboratory conditions. This is particularly vital for informing the design of robust control strategies, adaptive airframe configurations, and real-time gust mitigation systems. Understanding the response of flat plates at high sweep angles subjected to discrete vortex gusts thus fills a critical gap in current aerodynamic literature and offers direct practical value to next-generation flight vehicles operating in gust-rich environments.

The primary objective of this study is to experimentally investigate the aerodynamic response of a flat plate wing model with a 45° sweep angle when subjected to discrete vortex gusts. The scope of this work encompasses both quantitative flow visualization and aerodynamic force assessment, enabling a unified view of the fluid-structure interaction under unsteady gust environments. The results are expected to clarify the influence of sweep geometry, symmetry plane consideration, and tip geometry, thereby contributing to both fundamental understanding and the applied design of gust-resilient airframes, particularly for UAVs and other small-scale platforms operating in highly disturbed environments. To explore the unsteady aerodynamic response under controlled gust conditions, a series of water channel experiments are conducted using a gust generation mechanism. The gusts are generated via controlled rotational motion of a flat-plate gust generator, simulate localized, transient disturbances that resemble a discrete vortex gust phenomena. By varying key parameters such as the vertical distance between the gust generator and the wing (Δy) and the half-rotation duration of the generator (T), the study aims to systematically characterize how the gust encounter is affected by the vortex trajectory, and its propagation speed in terms of resulting forces and flow structures for a swept wing. Three distinct wing configurations are examined: a no-swept flat plate, a 45° swept flat plate, and a 45° swept plate with a sharp tip modification. For each configuration, multiple test cases are executed across two vortex trajectories (h/c), which are adjusted by varying Δy, and three half-rotation durations (T), resulting in a comprehensive test matrix made of 6 cases. Force measurements and Digital Particle Image Velocimetry (DPIV) analyses are conducted to quantify lift coefficients and vorticity fields. Reynolds number of 10,000 is maintained throughout all experiments. This experimental setup enables both high temporal resolution of aerodynamic loads and direct visualization of vortex-wing interaction mechanisms, forming a strong foundation to interprete the complex, transient flow phenomena associated with discrete vortex gust encounters.

Following the introductory section, the subsequent part of the study offers a detailed literature review and terminology background, encompassing key definitions related to gust dynamics, previous experimental and computational studies on gust encounters, and specific investigations concerning swept wings and discrete vortex interactions. This is followed by a complete explanation of the experimental methodology, including the water channel setup, gust generation system, model geometries, and instrumentation. The next section provides the investigated cases, and a comprehensive analysis of the experimental results, with particular focus on aerodynamic force trends, flow field visualizations, and the effects of sweep and gust parameters. The study concludes by summarizing the key findings and proposing directions for future research.

2. LITERATURE REVIEW

In recent decades, the aerodynamic community has placed significant emphasis on understanding how unsteady atmospheric conditions impact the performance and stability of flight vehicles, especially under gust encounters. In aerodynamics, gusts are localized, transient changes in wind velocity that generate unsteady aerodynamic loads on an aircraft. They are broadly categorized as continuous or discrete, with the latter producing rapid force and moment variations over short timescales. Discrete gusts can be further classified into (a) transverse gusts, where the velocity disturbance is perpendicular to the freestream; (b) streamwise gusts, where it is aligned with the freestream; and (c) vortex gusts, which consist of coherent swirling flow structures. Vortex gusts, which are often encountered near terrain irregularities, urban environments, or ship wakes, can induce highly nonlinear responses such as sudden lift changes, pitching moment fluctuations, and flow separation. For swept-wing configurations, gust characterization must also account for three-dimensional effects like spanwise phase variation and asymmetric vortex breakdown, which cannot be captured by two-dimensional models [1]. These discrete gusts are of particular interest due to their pronounced and instantaneous effects on airfoil loading, which is critical for the design and control of modern air vehicles operating in complex flow environments. Traditional approaches to gust modeling trace back to foundational works like those of Wagner [4] and Küssner [5], who proposed linearized analytical models for unsteady lift prediction due to step changes or ramp inputs in gust profiles. These models have since served as a baseline for understanding more complex gust phenomena. Moreover, the development of standardized gust profiles like the “1-cosine” profile reflects an industry-driven effort to replicate realistic atmospheric conditions within controlled simulations and experiments. Understanding these classifications and modeling techniques lays the groundwork for analyzing more complex gust-airfoil interaction phenomena, such as those involving three-dimensional geometries or vortex-dominated structures.

Early studies on gust-airfoil interactions predominantly relied on theoretical and analytical formulations. The study of von Kármán & Sears [6] laid the foundation for understanding airfoil responses to sinusoidal gust inputs through linear unsteady aerodynamics. This was followed by Küssner's step-function response model [5], which further enriched the theoretical framework for transverse gust interactions. Later, Adamczyk [7] presented an analytical investigation on the interaction of a swept wing with an oblique gust, highlighting the role of compressibility and three-dimensional effects in altering aerodynamic responses. These pioneering works collectively formed the theoretical underpinnings for later experimental and numerical investigations.

Subsequent research efforts transitioned from purely analytical models to experimental and computational approaches, especially utilizing flat plate models to isolate fundamental flow mechanisms. Perrotta & Jones [8] conducted experiments on large transverse gust interactions with flat plates, focusing on unsteady lift responses. Corkery et al. [9] developed a towing tank test rig to simulate transverse gust encounters, highlighting observations of vortex structures in the jet shear layers. Biler et al. [10] studied vortex and transverse gust encounters at low Reynolds numbers, offering insights into the influence of gust type, similarities in gust response and fundamental differences. Sedky et al. [11] compared sinusoidal and trapezoidal gust shapes, showing their differential impacts on transient lift forces. Gementzopoulos et al. [12] experimentally investigated large-amplitude transverse gust encounters using a flat plate wing and a wing with a symmetrical airfoil, demonstrating that the vorticity distributions shed from the leading and trailing edges govern the rise and fall of lift, and comparing their findings with Küssner's transverse gust model. In the numerical study of Badrya et al. [13], the unsteady aerodynamic response of a flat plate wing subjected to large-amplitude, sharp-edged transverse gusts, highlighting nonlinear effects in the transient lift evolution is investigated. Biler et al. [14] have further performed combined experimental and computational studies on flat plate wings encountering transverse gusts, enabling detailed validation of numerical predictions against measured flow structures and force histories. These works emphasized how simplified geometries, such as flat plates, serve as useful surrogates for more complex wings by enabling detailed flow measurements and validation of computational models.

Within the broader context of gust interaction research, vortex gusts have emerged as a particularly critical area of study due to their impact on aerodynamic surfaces. The work by Cem Gözükara et al. [15] analyzed discrete vortex gust effects on flat plates using experimental and numerical methods, highlighting discrepancies and agreements between computational predictions and measurements. Soy et al. [16] investigated the transition from discrete to continuous vortex gusts, capturing the intermediate regimes that blend isolated and periodic characteristics. Qian et al. [17] extended this exploration by examining three-dimensional effects in vortex gust interactions with finite wings, utilizing PIV measurements to analyze spanwise lift distribution. Their study offered deeper insights into the structural deformation and diffusion of vortex filaments during interaction, showcasing time-resolved aerodynamic force measurements. Riddle et al. [18] used numerical simulations to study vortex trapping on swept wings, identifying mechanisms for vortex attachment and separation as influenced by local pressure gradients. Zhu & Breuer [19] explored pitch-induced vortex dynamics on swept wings, linking vortex behavior to aeroelastic instabilities such as limit-cycle oscillations. Vadher & Babinsky [20] focused on the controlled generation of vortex gusts, a foundational aspect for reproducible gust encounter experiments. Ito et al. [21] examined the role of vortex generators on transonic swept wings, drawing parallels to vortex-induced loading seen in subsonic gust interactions. Collectively, these studies provide a comprehensive understanding of vortex-induced aerodynamic loads and set the stage for three-dimensional exploration.

The increasing recognition of spanwise and chordwise variations in gust responses has led to a surge in studies emphasizing the need for three-dimensional modeling. Qian et al. [17] demonstrated that swept wings exhibit notable spanwise independence in vortex loading, emphasizing the importance of capturing three-dimensional flow structures. Wild & Jones [22] further highlighted the implications of sideslip and three-dimensionality in transverse gust encounters, reinforcing the necessity of moving beyond two-dimensional simplifications. These findings collectively argue for the inclusion of realistic three-dimensional effects when modeling gust encounters in modern flight scenarios.

Given the complex flow phenomena associated with three-dimensional wings, especially those with sweep, researchers have conducted targeted investigations on swept wing-gust interactions. Adamczyk's early analytical model [7] served as a theoretical foundation, while Qian et al. [17] provided experimental verification using PIV measurements on finite swept wings. Zhu & Breuer's [19] study emphasized the role of sweep in modulating vortex-induced lift fluctuations, showing how geometry influences unsteady aerodynamics. Riddle et al. [18] contributed with numerical findings on vortex trapping, particularly relevant for high sweep angles. Finally, Wild et al. [3] discussed three-dimensional gust effects on swept wings under strong transverse conditions, capturing the compounded influence of sideslip and planform geometry. These works collectively bridge the gap between theoretical predictions and practical applications involving swept configurations.

In the context of benchmark comparisons, two studies have played a central role in informing the experimental design and configuration choices of the present work. The study by Yilmaz & Rockwell [23] analyzed flow structures on a three-dimensional swept wing subjected to small amplitude perturbations. Notably, their experimental setup did not employ a perfect half-span model, but instead included 15% of the mirrored side of the wing beyond the symmetry axis. This configuration served as the foundation for our own partially V-shaped wing experiments, which aim to evaluate the aerodynamic implications of including such a mirrored section. Similarly, the work by Wild et al. [3] examined transverse gust interactions on swept wings by adjusting the sideslip angle of a rectangular wing, resulting a misalligned tip geometry (sharp-tip) with the freestream. Inspired by their findings, we incorporated both misaligned and aligned tip configurations into our experimental campaign, enabling a direct comparison of tip geometry effects under equivalent gust conditions.

The present work offers several unique contributions to the field. First, by comparing between no-swept and swept wing configurations to reveal the effect of sweep angle. Second, by systematically comparing half-span and partially mirrored V-shaped swept wing models, we explore the aerodynamic influence of mirroring and symmetry conditions in isolation. Third, building on the inspiration from the study of Wild et al. [3], we analyze the role of tip geometry in modulating unsteady aerodynamic forces, using identical experimental conditions for misaligned and aligned tips with the freestream. Lastly, our study incorporates detailed time-resolved force measurements and flow viusalization results that reveal phase lags in aerodynamic response across different wing configurations. These temporal shifts, which termed as "time shifts", highlight previously underexplored dynamic behaviors and contribute novel insights into the vortex gust interaction problem, extending the body of knowledge in both experimental methodology and aerodynamic theory.

3. EXPERIMENTAL SETUP

3.1 Flow System

The experiments are conducted in a closed-loop, free-surface water channel located in the Trisonic Research Laboratory at the Faculty of Aeronautics and Astronautics, Istanbul Technical University. The water channel includes an inlet reservoir followed by a flow straightening section that consists of a honeycomb and five screens. This arrangement aims to achieve a uniform flow with low turbulence intensity. Subsequently, a contraction section accelerates the flow, with a contraction ratio of 2. The test section, constructed with plexiglass walls (two sides and the bottom), allows for optical access necessary for flow visualization via Digital Particle Image Velocimetry (DPIV).

The test section has a width of 1010 mm and a height of 790 mm. The free-stream velocity is controlled by the motor's RPM via an ABB AC Drive. The experiments are conducted at a free-stream velocity of 0.1 m/s, corresponding to a Reynolds number of 10,000 based on the chord length of the wing model.

3.2 Test Models

To generate the vortex gust, a flat plate model, referred to as the gust generator, is fabricated. This gust generator has a wingspan of 400 mm and a chord of 100 mm, with both leading and trailing edges sharpened at a 45° wedge angle. It has 5 mm thickness and constructed from plexiglass.

Three wing models are tested downstream of the gust generator:

- **No-Swept Flat Plate:** A rectangular wing model with 0° sweep angle, made of 5 mm thick plexiglass. It has a chord of 100 mm and a span of 200 mm. As the experiments are conducted in a free-surface water channel, the model is, representing a semi-span configuration. Hence, the effective aspect ratio of the model is 4.

- **45° Swept Wing:** This model also has a 100 mm chord and 200 mm span. This model included an additional segment on the opposite side of the root (above the waterline) extending 15% of the full span (30 mm), forming a partial V-shaped planform. The model is tested in two sub-configurations: (i) when the free surface intersects the model at its root chord (symmetry axis), and (ii) when the water level is raised to include the 15% extra portion.
- **Sharp-Tip 45° Swept Wing:** Similar in dimensions and planform to the previous swept model, this variant features a sharp tip created by 90° bends between the leading edge, tip, and trailing edge. It also has a 15% span extension mirrored across the symmetry plane. Again, two sub-configurations are considered with different immersion depths.

The schematic representations of the wing models and their corresponding configurations are provided in Figure 3.1.

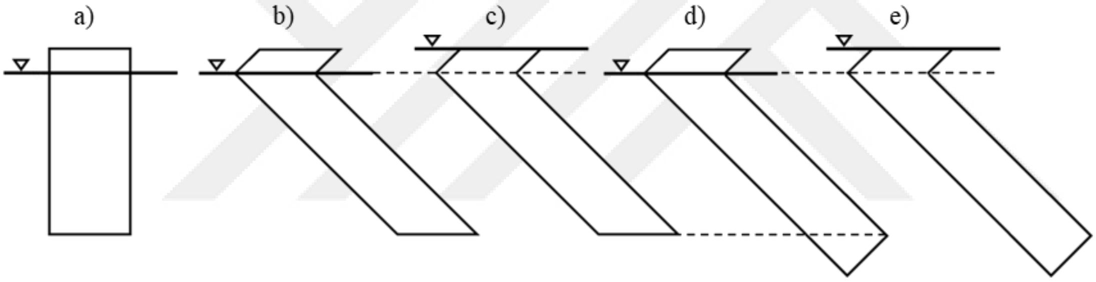

Figure 3.1 : Wing model configurations, a) No-swept, b) 45° Swept, c) 45° Swept (including 15% of the opposite side of symmetry axis), d) Sharp-Tip 45° Swept, e) Sharp-Tip 45° Swept (including 15% of the opposite side of symmetry axis).

The gust generator and wing models are mounted from above the free surface in a cantilevered arrangement using servo-driven rods. The horizontal distance between the gust generator's trailing edge and the root leading edge of the wing model, denoted as Δx, is fixed at 58 mm for all configurations. The vertical offset between the gust generator and the wing model, denoted as Δy, is one of the major parameters in the study to control vortex trajectory height with respect to the wing chordline.

Both the gust generator and wing models are connected to Kollmorgen/Danaher Motion servo motors via vertical rods. The gust generator is attached at the mid-chord point and undergoes a 180° clockwise rotation during each test. The wing models are mounted at their root leading edge, with the servo connection passing through a six-component force/torque sensor, detailed in Section 3.4.

The rotational motion of the gust generator can be seen in Figure 3.2, which also illustrates the relative location of Δy, Δx, and vortex trajectory height (h).

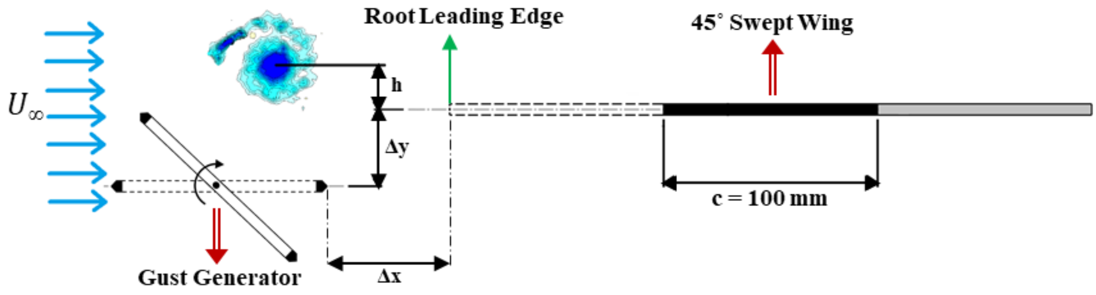

Figure 3.2 : Camera view (test section bottom view) of the gust generator and the wing model.

Additional details regarding the laser sheet locations and water free surface are provided in Figure 3.3, which illustrates the planform view of the swept wing with dimensional annotations.

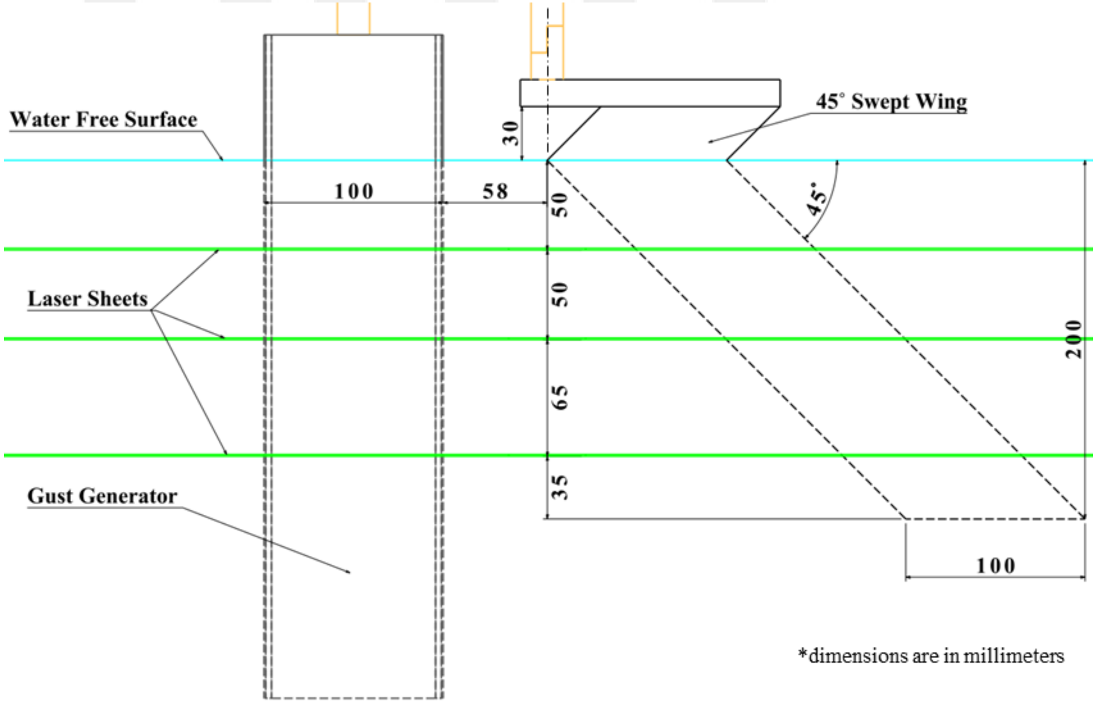

Figure 3.3 : Planform view of the swept wing and the gust generator, and illuminated planes positioning.

3.3 Quantitative Imaging System

Quantitative flow field measurements are conducted using a Digital Particle Image Velocimetry (DPIV) system. The measurement plane is illuminated by a dual-cavity Nd:YAG laser with a maximum energy output of 120 mJ/pulse. Polyamid Seeding Particles (PSP) with an average diameter of 50 µm are used to seed the flow.

Two 10-bit FlowSense cameras with a resolution of 1600×1200 pixels and 35 mm Nikon lenses were mounted beneath the test section, aligned perpendicular to the illuminated plane. The relative positioning of the cameras, laser system, gust generator, and wing model within the test section is illustrated in Figure 3.4.

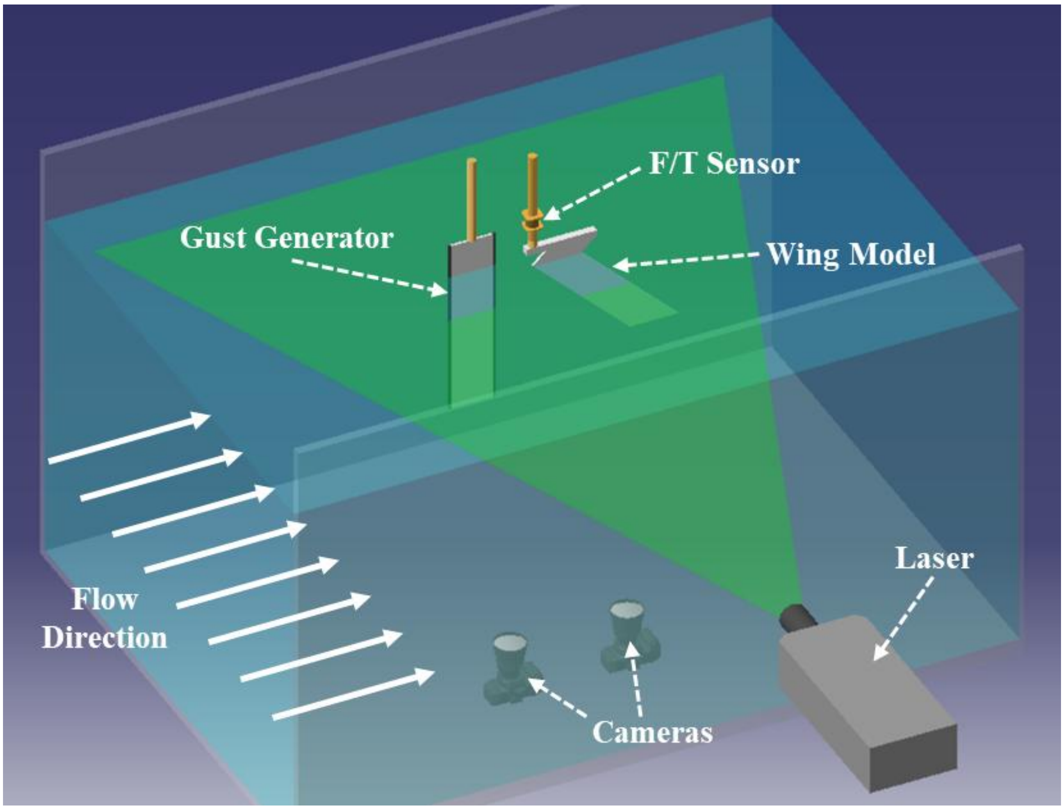

Figure 3.4 : Experimental setup.

The use of two cameras is essential due to the large streamwise field of view required by the 45° swept wing. The cameras are placed side by side, aligned along the streamwise direction, with overlapping regions to enable image stitching. Images are acquired at a rate of 10 Hz with a time between pulses of 7500 µs. For each test case, 300 image pairs are recorded.

Image acquisition and post-processing are carried out in Dantec Dynamic Studio (v4.10.67). Prior to post-processing, the stitched field is generated using the MATLAB Link Tool in Dynamic Studio. Following this, the gust generator and wing model are masked, and Adaptive PIV algorithm is used to apply cross-correlation method. It starts with a minimum interrogation area of 32×32 pixels and goes up to maximum 128×128 pixels with 16-pixel grid step size. Vector validation methods of range validation and moving average validation are employed, and coherence filtering is applied to the data.

Each case is repeated five times to improve data reliability. The resulting velocity fields from these repetitions are averaged to reduce noise. Vorticity are then computed from the final averaged data by using scalar derivatives.

All DPIV measurements are performed simultaneously with force measurements using a LabVIEW-based control and synchronization system. This system triggered the laser, cameras, force acquisition module, and the servo motor responsible for rotation of gust generator via a single synchronized signal, ensuring temporal alignment between flow field data and aerodynamic force measurements.

3.4 Force Measurement System

For time-resolved force and moment measurements, a six-component ATI NANO-25 Force/Torque sensor is utilized. The sensor is placed between the wing's connection rod and the vertical extension connected to the servo motor. The connection rod passes through the wing root leading edge, ensuring alignment with the spanwise (z-axis) direction. This arrangement can be seen in Figure 3.4 and indirectly in the technical drawing of the swept wing (see Section 3.2).

The sensor operates at a sampling frequency of 1000 Hz. Each test is repeated five times, and the resulting force signals are averaged. Additionally, a 1 Hz low-pass filter is applied to reduce the noise. The sensor provides a resolution of 1/24 N and, based on prior studies [24], has a maximum uncertainty of 0.2083 in lift force coefficient measurement.

As the DPIV measurements are performed at three different spanwise locations, the entire set of test cases are repeated independently for each measurement plane. Although this resulted in 15 total repetitions per case, the averaging is performed separately within each group of five runs to preserve consistency. The similarity of results across all three planes demonstrated the repeatability of the measurements. Further discussion of this approach is provided in the Results chapter under the Investigated Cases section.

4. RESULTS

4.1 Investigated Cases

In this study, two main parameters are systematically varied to construct a test matrix for analyzing the interaction between a large scale discrete vortex gust and the wing. The first parameter is the vertical distance between the gust generator and the wing, denoted as Δy, which directly affects the trajectory height of the generated vortex with respect to the wing chordline. The second parameter is the half rotation duration of the gust generator, denoted as T, representing the time required for a 180° rotation and affecting the propagation speed of the vortex gust [25].

Two different vertical distances are tested: $\Delta y = -36mm$ and $\Delta y = -111mm$. These correspond to non-dimensional trajectory heights of $h/c=0$ and $h/c=-0.75$, respectively. Regarding the second parameter, three different half rotation durations are used: $T = 3s, 4s, 6s$. Each test case is defined by a unique combination of Δy and T, and repeated five times. A summary of all parameter combinations is provided in Table 4.1.

Table 4.1 : Test matrix.

Δy (mm)	h (mm)	h/c	T (s) (1/2 rotation)
−36	0	0	3 4 6
−111	−75	−0.75	3 4 6

Each of the six test cases is carried out for five different wing configurations. As introduced in Section 3.2, three distinct flat plate models are used: a no-swept wing, a 45° swept wing with a sharp tip, and a 45° swept wing with a tip aligned with the freestream direction. For the two swept wing geometries, two water surface levels are considered. In one of the scenarios, the water free surface intersects the wing at its root chord plane, while in the other, the water level is elevated to include the outer 15%

spanwise extension of the wing, producing an appearance similar to a partial V-shape. Altogether, five wing configurations are tested across all six test cases.

The comparison of results includes both the time-varying aerodynamic loads and the instantaneous flow field structures during vortex interaction. First, the no-swept wing is compared against the 45° swept wing with flow-aligned-tip tested under the configuration where the water free surface aligns with the root chord plane. Following this, the effect of the water free surface level is investigated for the two swept-wing geometries, which are the flow-aligned-tip and sharp-tip configurations, by comparing the aerodynamic and flow responses between their respective water levels. Lastly, to evaluate the influence of tip geometry, results from the sharp-tip and flow-aligned-tip swept wings are compared under the same water surface condition.

Flow visualization is performed through three illuminated planes distributed along the spanwise direction of the wing. While the positions of these planes vary along the span (*z*-direction), the planes themselves are oriented perpendicular to the spanwise axis and parallel to the freestream (i.e., parallel to the *xy*-plane). The same three planes are used across all wing configurations and cases, and each time the illuminated plane is changed, all six test cases are independently repeated five times, resulting in a total of 15 repetitions per configuration. This consistency ensures reliable comparison of force measurements across models and setups.

The nondimensional spanwise location of each illuminated plane is defined by η as;

$$\eta = \frac{z}{s/2} \tag{4.1}$$

where *z* is the spanwise distance from the symmetry plane and *s* is the full wingspan. Measurements are acquired at $\eta=0.25$, $\eta=0.5$, and $\eta=0.825$, as shown in Figure 4.1.

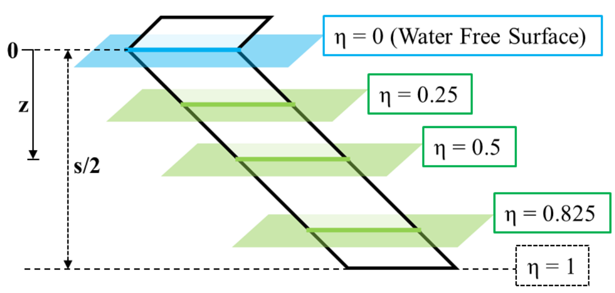

Figure 4.1 : Spanwise positions of illuminated planes (shown as green).

Although the layout is illustrated on the 45° swept wing with flow-aligned-tip, the same η positions are maintained for all other configurations.

4.2 Force Measurement and PIV Results

This section presents a comparative analysis of the aerodynamic force responses and flow visualization results obtained from the interaction between the generated vortex and different wing configurations. The comparisons are structured into three main subsections based on the specific configuration differences explored: (i) sweep angle effect, (ii) free surface level effect, and (iii) tip geometry effect.

For each case and each illuminated plane, the force measurements from five repeated runs are post-processed by extracting the mean response from each set of five runs. These three mean curves (repeated each time the illuminated plane changes) are then visualized together without averaging them further. This is intentionally done to highlight the repeatability of the experiment across different days.

The plots of aerodynamic response over convective time (t^*) are presented in terms of the lift transient (ΔC_L), where the convective time defined as:

$$t^* = \frac{t \cdot U_\infty}{c} \tag{4.2}$$

Here, t is the physical time, U_∞ is the freestream velocity, and c is the chord length. In the current experiments, $U_\infty = 0.1\ m/s$ and $c = 0.1\ m$, leading to $t^* = t$. The motion of the gust generator starts at $t^* = 0$.

It should be noted that in previous studies [15, 17], the case of $T = 4s$, $\Delta y = -36mm$ is considered as the base case which considers a vortex trajectory aligned with the chordline of the no-swept wing.

The following subsections focus on configuration-specific comparisons while building upon the shared framework described above.

4.2.1 Sweep effect

The first comparison aims to explore the influence of wing sweep on the transient aerodynamic loads and the resulting flow structures. For this purpose, a no-swept (rectangular) wing is compared against the 45° swept wing tested under the configuration where the water free surface coincides with the root chord plane of the swept wing. In this arrangement, the submerged span of both models remains identical, thus enabling a direct comparison of sweep-induced effects.

4.2.1.1 The case of h/c = 0 (Δy = −36mm)

Figure 4.2 displays the lift transient responses for the no-swept and 45° swept wing configurations under the scenario of $\Delta y = -36mm$, corresponding to $h/c = 0$. Each curve represents the lift transient variation for a given half rotation duration T.

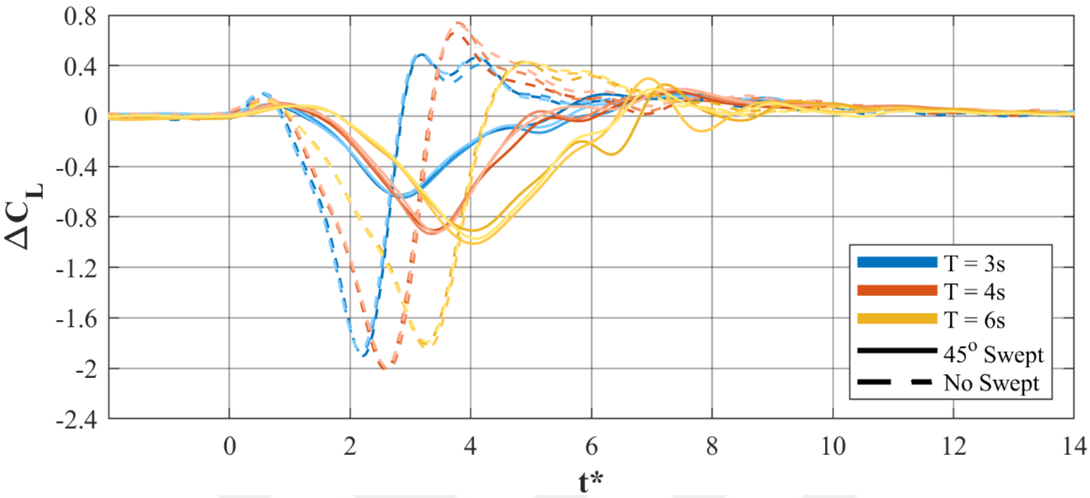

Figure 4.2 : Comparison of ΔC_L between no-swept wing and 45° swept wing configurations for $h/c = 0$.

A common trend, as can be seen in Figure 4.2, is that the lift transient occurs later in time across both configurations. This behavior is evident from the rightward shift of the negative major peaks in time as the gust generator rotates more slowly, delaying the vortex impingement.

This trend persists across both configurations; however, the presence of sweep further delays the lift response for each T case. The PIV-based vorticity fields shown in Figures 4.3 to 4.5 provide further insight into these observations. Each figure corresponds to one of the three gust generator half-rotation durations ($T = 4s$, $3s$, and $6s$), and presents a side-by-side comparison of the flow structures near the wing at their respective negative peak instants between no-swept wing on the left and 45° swept wing on the right.

For the case of $T = 4s$ with $h/c = 0$ (Figure 4.3), the negative peak of the ΔC_L occurs at $t^* = 2.6$ for the no-swept configuration, whereas this moment is delayed to $t^* = 3.4$ for the 45° swept wing. Despite the temporal offset, both configurations display a qualitatively similar vortex structure near the wing at their respective minimum instants, which is characterized by the negative vortex gust interacting positive leading edge vortex, particularly around the root section.

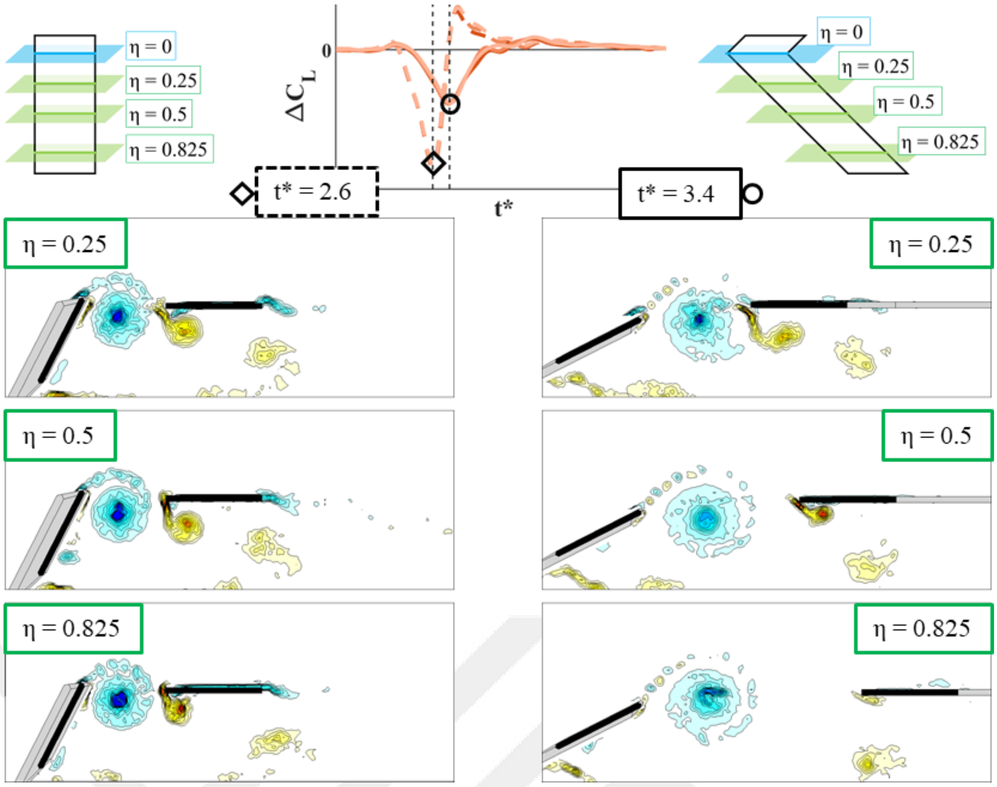

Figure 4.3 : Comparison of vorticity distributions between no-swept wing and 45° swept wing for the case of *T = 4s* and *h/c = 0*, at the moment of major negative peak of the lift transient.

For the case of *T = 3s* with *h/c = 0*, Figure 4.4 shows a similar temporal pattern, where the negative peak of the ΔC_L occurs at *t* = 2.2* for the no-swept and at *t* = 2.8* for the 45° swept configuration. Again, the positive vortex structure induced on the swept wing (the leading-edge vortex) is observed later compared to that of the no-swept counterpart.

In Figure 4.5, for the case of *T = 6s* with *h/c = 0*, the occurance of the major negative peak of ΔC_L shifts in time from *t* = 3.3* in the no-swept case to *t* = 4.0* in the swept case. While the vortex structure from the gust generator continues to exhibit near-identical characteristics, the induced LEV on the swept wing again forms later compared to that of the no-swept wing configuration. This reinforces the interpretation that the sweep introduces a temporal shift in the aerodynamic response.

Furthermore, this delay is not only visible in the overall lift response but also in the sectional development of the induced flow structures. For the swept wing, the LEV developement near the root appears earlier than it does at other sections. In other words, the phase shift in aerodynamic response is further reflected spanwise,

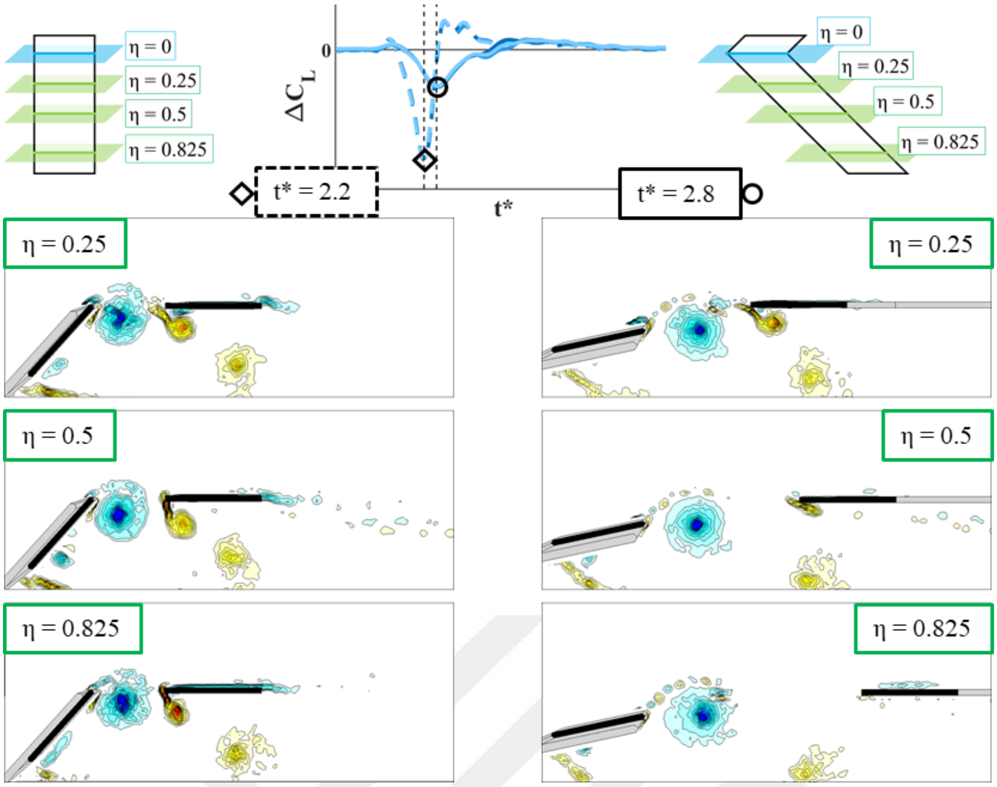

Figure 4.4 : Comparison of vorticity distributions between no-swept wing and 45° swept wing for the case of *T* = *3s* and *h/c* = *0*, at the moment of major negative peak of the lift transient.

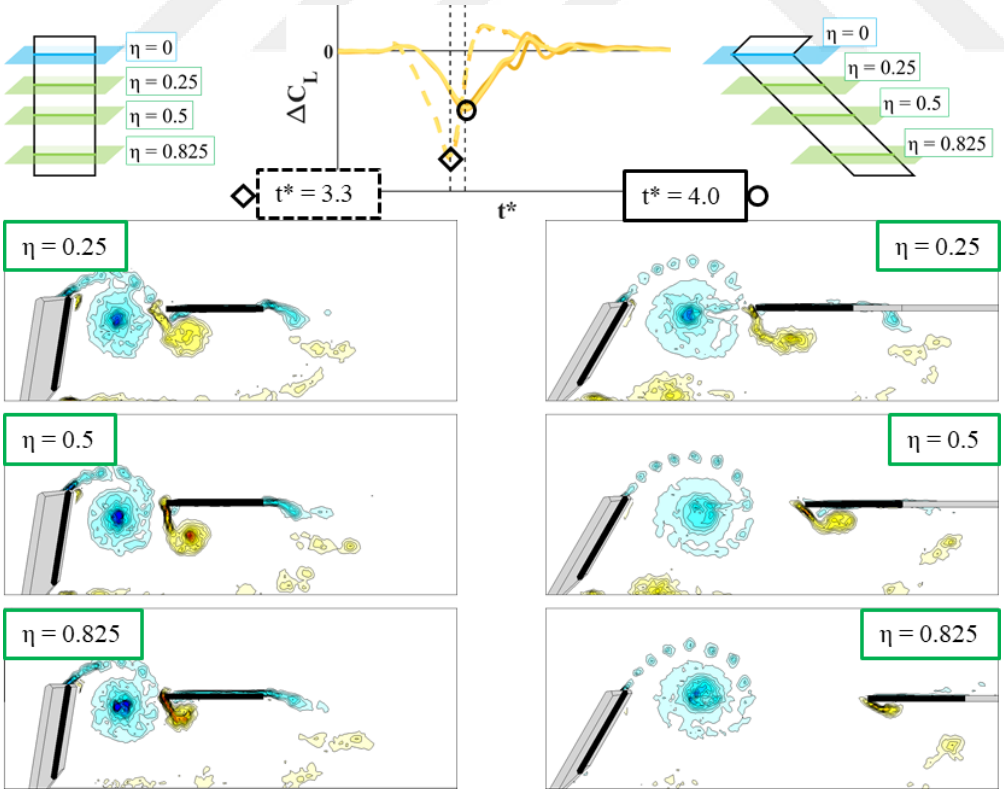

Figure 4.5 : Comparison of vorticity distributions between no-swept wing and 45° swept wing for the case of *T* = *6s* and *h/c* = *0*, at the moment of major negative peak of the lift transient.

as the similar vortex pattern emerges progressively later from the root toward the tip due to the geometric sweep of the wing. This spanwise temporal progression, caused by geometric sweep, reflects the three-dimensional nature of the interaction and highlights how the response propagates in a staggered fashion.

This spanwise temporal shift in vortex development, which is evident both in the lift response and in the flow structures across sections, should be noted as a key observation since it forms the basis for a further discussion that will be revisited toward the end of this chapter.

4.2.1.2 The case of h/c = −0.75 (Δy = −111mm)

Figure 4.6 shows the lift transient responses for the no-swept wing and 45° swept wing when the vortex encounters the wing at a trajectory height of $h/c = -0.75$.

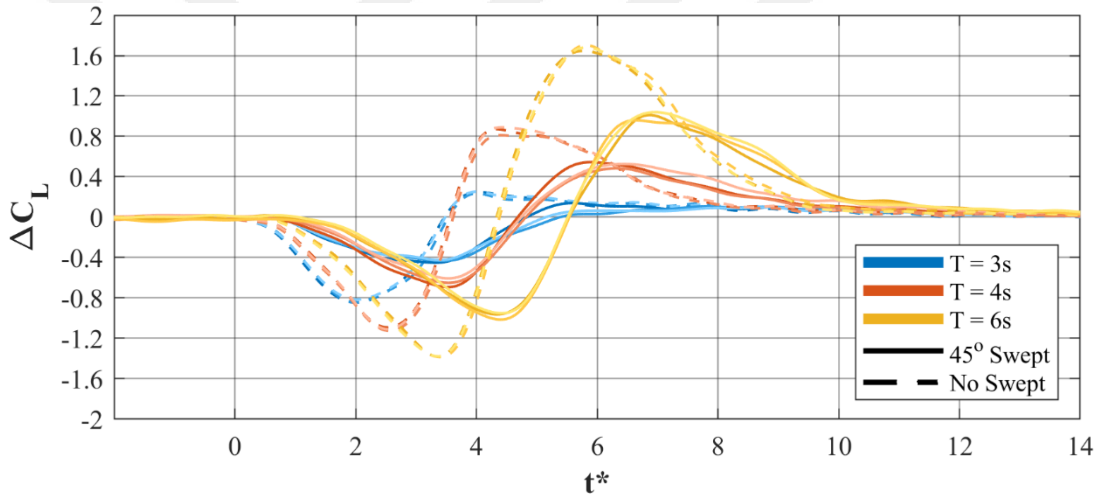

Figure 4.6 : Comparison of ΔC_L between no-swept wing and 45° swept wing configurations for $h/c = -0.75$.

Compared to the previous case with $h/c = 0$, the vortex gust encounters the wing from below the chordline, resulting in a weaker interaction between the vortex and the wing. As a result, the magnitude of the negative peaks in ΔC_L is reduced for both configurations. Nevertheless, the same phase delay trend observed in the $h/c = 0$ case remains consistent: as the half-rotation duration T increases, the lift transient shifts toward later times, and the swept configuration continues to exhibit a more delayed and reduced response compared to the no-swept wing case.

Figure 4.7 presents the instantaneous vorticity contours at the major negative peak instants for $T = 4s$ with non-dimensional vortex trajectory of $h/c = -0.75$. For this case, the minimum ΔC_L occurs at $t^* = 2.6$ for the no-swept wing and at $t^* = 3.6$ for

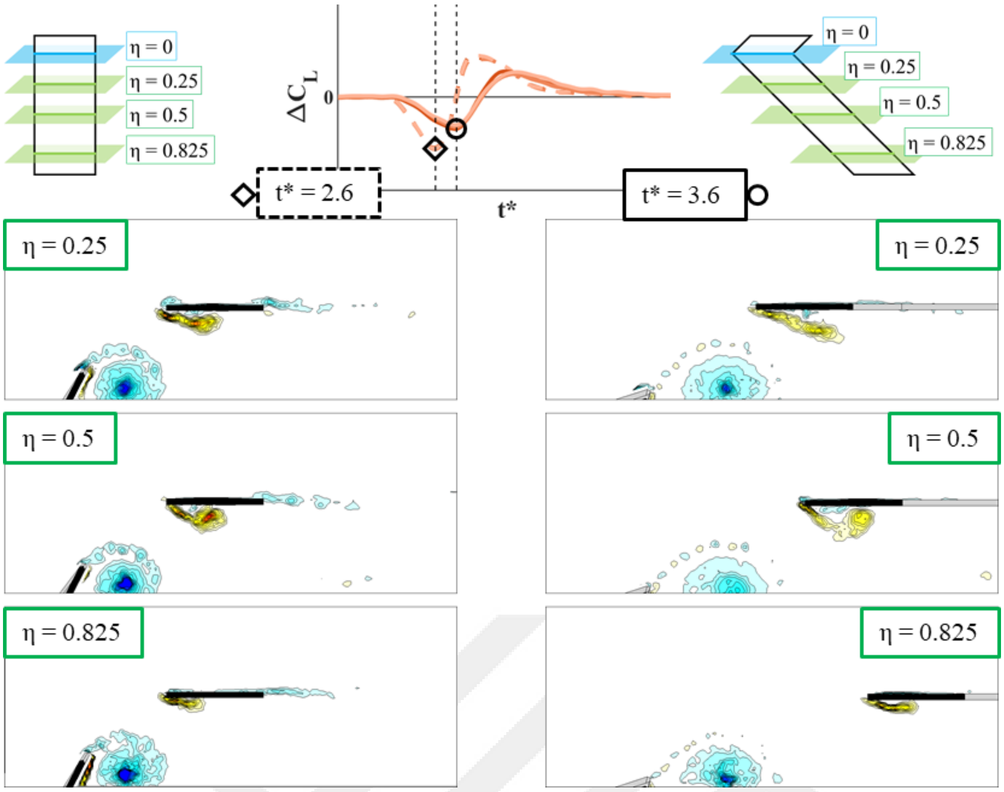

Figure 4.7 : Comparison of vorticity distributions between no-swept wing and 45° swept wing for the case of T = *4s* with $h/c = -0.75$, at the moment of major negative peak of the lift transient.

the swept wing. At these instants, the generated vortex has descended past the wing, and although it no longer strongly impinges on the surface, a negative effect is still induced. For the no-swept case, the leading-edge vortex structure is more compact. In contrast, the swept configuration shows a more separated and delayed formation of the positive LEV.

For $T = 3s$ with $h/c = -0.75$, the flow fields corresponding to the negative peak instants are displayed in Figure 4.8. The minimum ΔC_L is observed at $t^* = 2.0$ for the no-swept wing and at $t^* = 3.4$ for the swept wing case. The positive LEV in the no-swept case remains relatively attached to the surface, while in the swept configuration, the induced vortex appears more detached and slightly weaker in structure.

Similarly, Figure 4.9 compares the vorticity structures at the peak negative ΔC_L instants for $T = 6s$ with $h/c = -0.75$. Here, the negative peak of ΔC_L occur at $t^* = 3.4$ and $t^* = 4.4$ for the no-swept and swept cases, respectively. The vortex strength and alignment relative to the wing maintain similar patterns for both configurations, supporting the observation that the temporal delay and reduction in force magnitude come from the geometric sweep effect on the vortex-wing interaction.

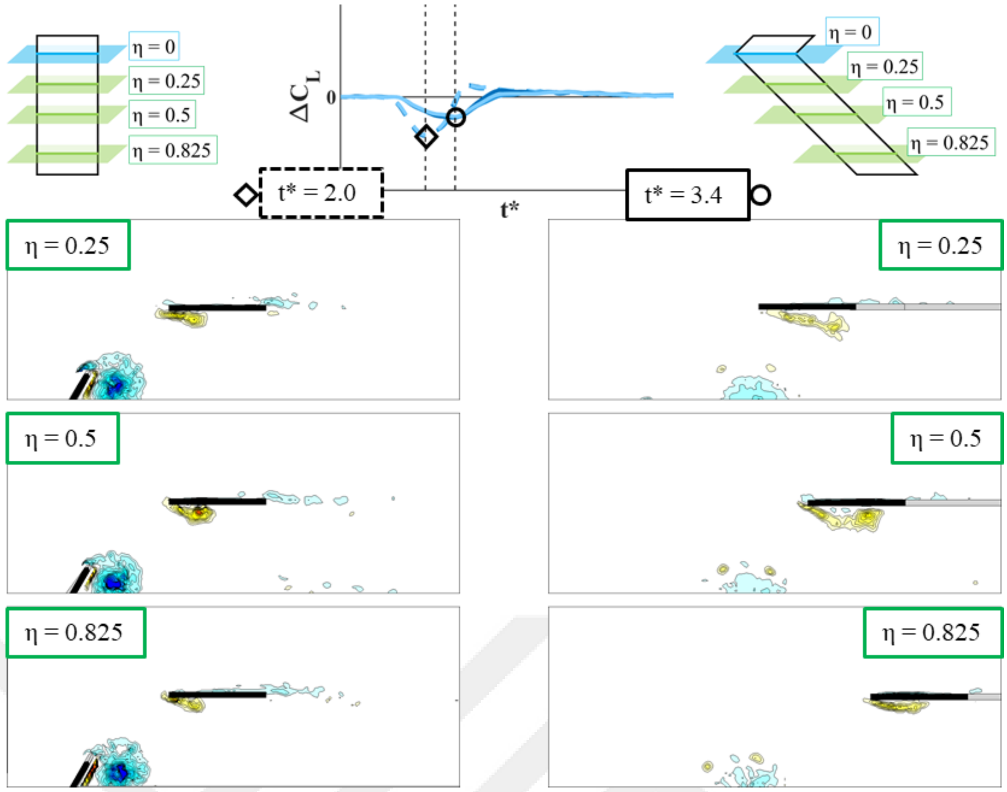

Figure 4.8 : Comparison of vorticity distributions between no-swept wing and 45° swept wing for the case of T = *3s* with h/c = *−0.75*, at the moment of major negative peak of the lift transient.

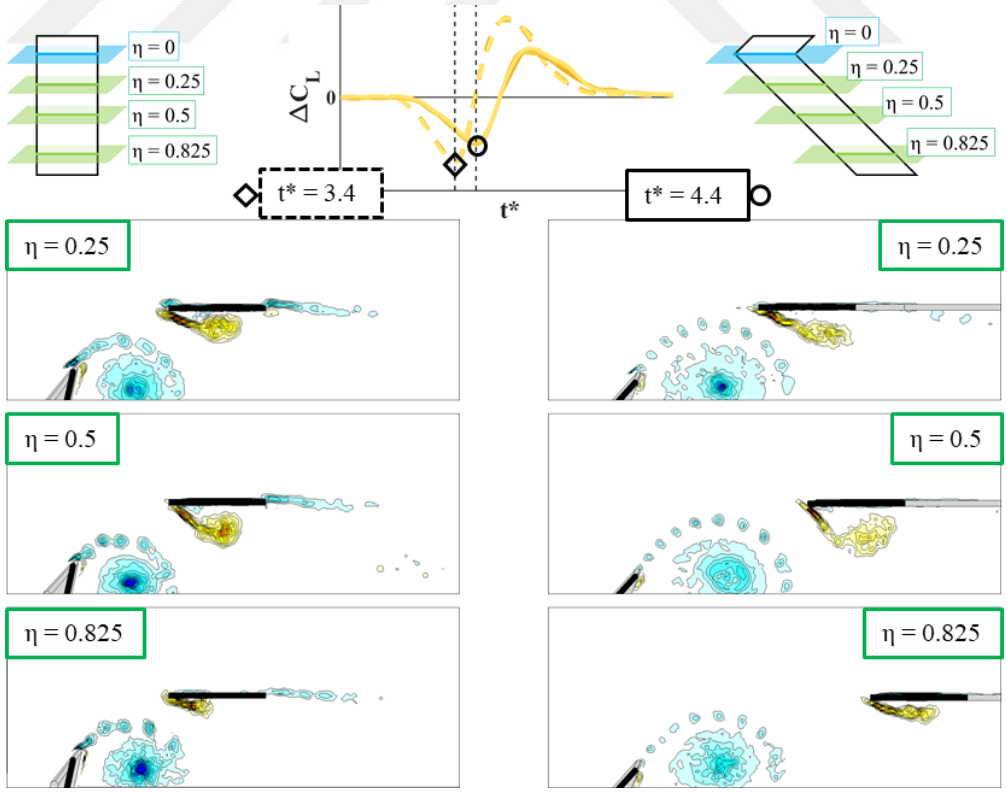

Figure 4.9 : Comparison of vorticity distributions between no-swept wing and 45° swept wing for the case of T = *6s* with h/c = *−0.75*, at the moment of major negative peak of the lift transient.

Notably, for the swept configuration, the induced leading-edge vortex patterns show a clear spanwise progression. At root sections, the response occurs earlier and with stronger coherence, while at mid and tip sections, similar structures emerge later in time with more diffused patterns. This observation supports the notion that the geometric sweep leads to a spanwise-delayed interaction.

4.2.2 Water level effect

As previously mentioned in Section 4.1, the free-surface level in the water channel was varied to examine its potential impact on the lift transient and flow structure. This variation effectively changes the intersection of the water surface with the wing span, resulting in two configurations for the 45° swept wing as one where the water level aligns with the root chord plane ($\eta = 0$), and another where it intersects above the root ($\eta = -0.15$). This modification corresponds to adding 15% of the half-span as additional submerged wing area. While the wing geometry remains constant, this adjustment results in a partially V-shaped submerged planform compared to the flat configuration. The potential influence of this difference is evaluated at zero angle of attack, which is the test condition used in all cases presented.

Figure 4.10 and Figure 4.11 present the lift coefficient responses for the $\Delta y = -36mm$ and $\Delta y = -111mm$ configurations, respectively. Each plot compares the lift transients of the swept wing for three different T values, tested under both water level settings. As clearly illustrated in both figures, the variation in free-surface elevation does not cause any meaningful deviation in the lift response. The curves corresponding to different water levels nearly overlap for each case, indicating that the additional submerged span due to the raised water surface does not influence the lift transient, at least under zero-angle-of-attack conditions.

To further confirm this observation, Figures 4.12 and 4.13 provide side-by-side comparisons of the vorticity fields for the two water level settings, based on the base case configuration ($\Delta y = -36mm$, $T = 4s$). Figure 4.12 corresponds to the minimum lift instant, while Figure 4.13 represents a later phase where the lift has returned to a positive value. In both cases, the flow structures remain nearly identical across all illuminated spanwise sections ($\eta = 0.25, 0.5,$ and 0.825). The vortex approaching from the gust generator maintains the same core size, position, and trajectory, while the counter rotating leading-edge vortex also shows no noticeable differences between the two water levels. Even in the later phase depicted in Figure 4.13, where the flow becomes highly three-dimensional and complex, the similarity in the vortex structures persists.

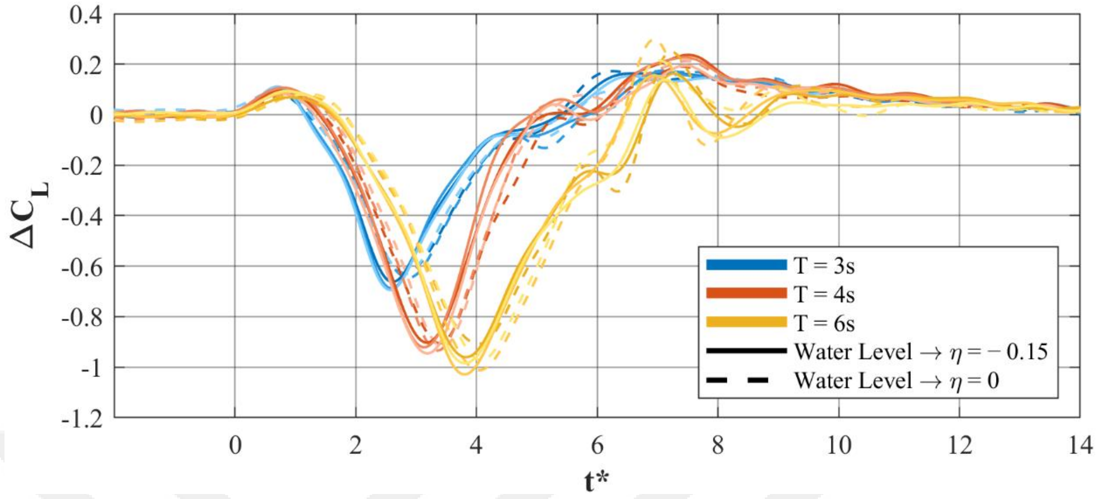

Figure 4.10 : Water level effect on ΔC_L for the case of $h/c = 0$, for 45° swept wing.

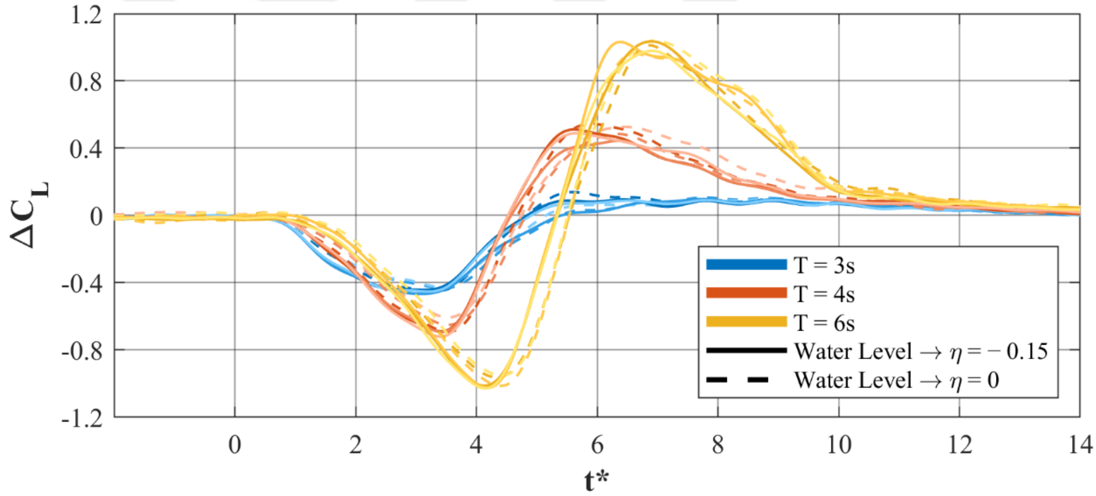

Figure 4.11 : Water level effect on ΔC_L for the case of $h/c = -0.75$, for 45° swept wing.

These results clearly demonstrate that altering the free-surface elevation has no significant influence on either the unsteady lift generation or the detailed vortex dynamics, at least for the present zero-angle-of-attack condition. It should be noted, however, that this conclusion is specific to the current test conditions. Under non-zero angle of attack, the added submerged area could potentially alter the aerodynamic response. This consideration is important when extrapolating the current findings to more general cases.

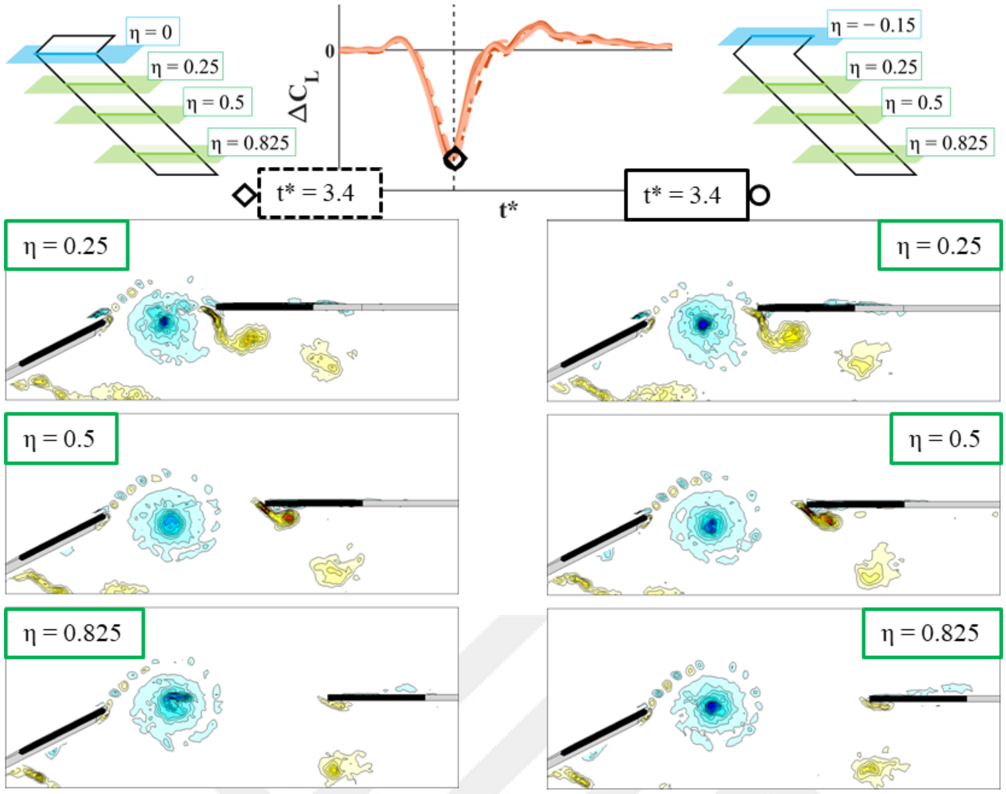

Figure 4.12 : Water level effect on flow structure for the case of *T = 4s* with *h/c = 0*, for 45° swept wing, at *t* = 3.4*.

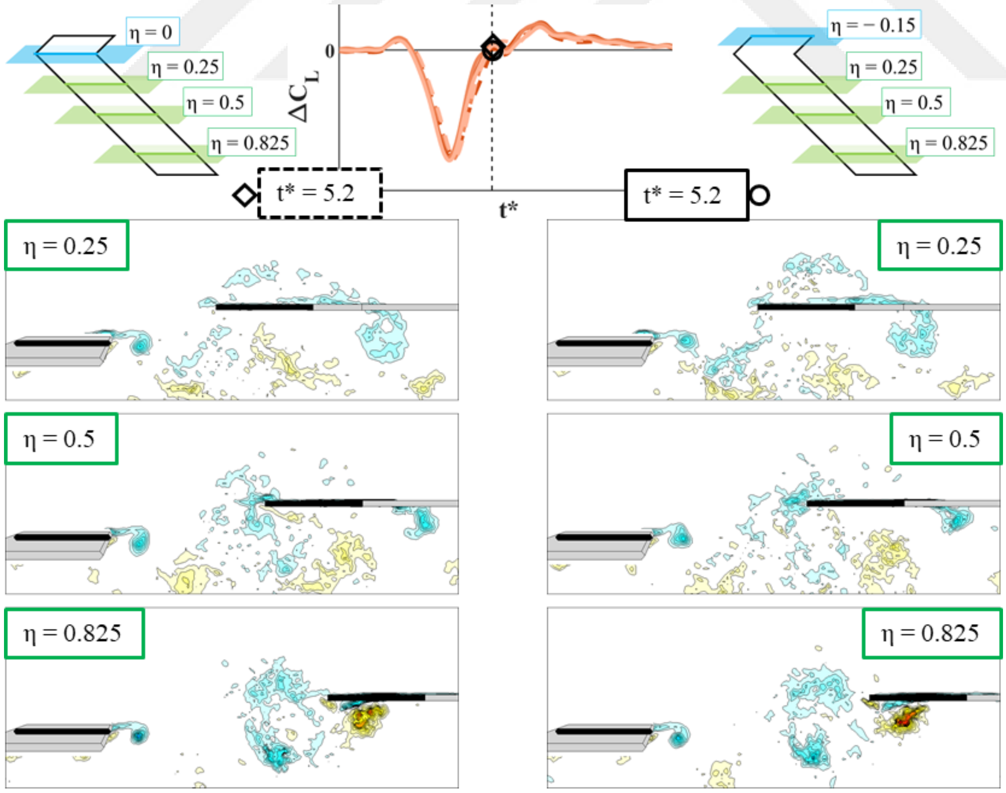

Figure 4.13 : Water level effect on flow structure for the case of *T = 4s* with *h/c = 0*, for 45° swept wing, at *t* = 5.2*.

Although the comparisons provided here are limited to the base case (*Δy = –36mm*, *T = 4s*) and 45° swept wing with aligned tip configuration, similar results were also observed for all the other cases and other swept wing configurations. For the sake of brevity, the corresponding plots are not presented, but the findings are consistent: the elevation of the water surface does not introduce any noticeable variation in force or flow behavior.

4.2.3 Tip geometry effect

Another geometric parameter investigated is the tip design of the swept wing. In this context, two 45° swept wing configurations were compared: one with an aligned tip shape (aligned with the flow direction), and another with a rectangular, sharp-edged tip. For both configurations, the water level was kept aligned with the root chord plane ($\eta = 0$).

The lift response for both configurations is presented in Figure 4.14 and Figure 4.15 for *Δy = –36mm* and *–111mm*, respectively. As clearly shown, the difference in tip geometry does not result in a significant change in the aerodynamic loading. The ΔC_L curves show nearly identical profiles across all cases, with matching minimum values, response timings, and post-minimum behaviors.

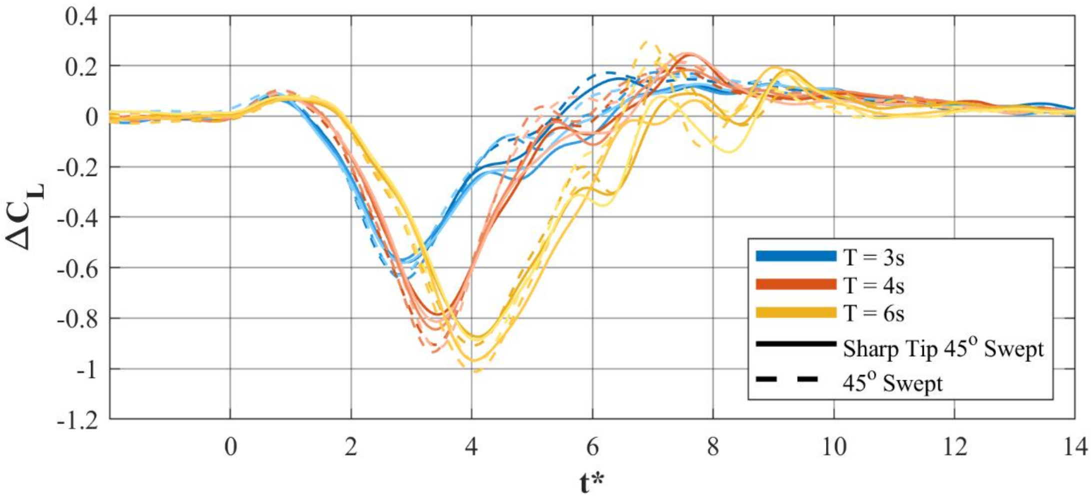

Figure 4.14 : Tip geometry effect on ΔC_L for the case of $h/c = 0$, for 45° swept wing.

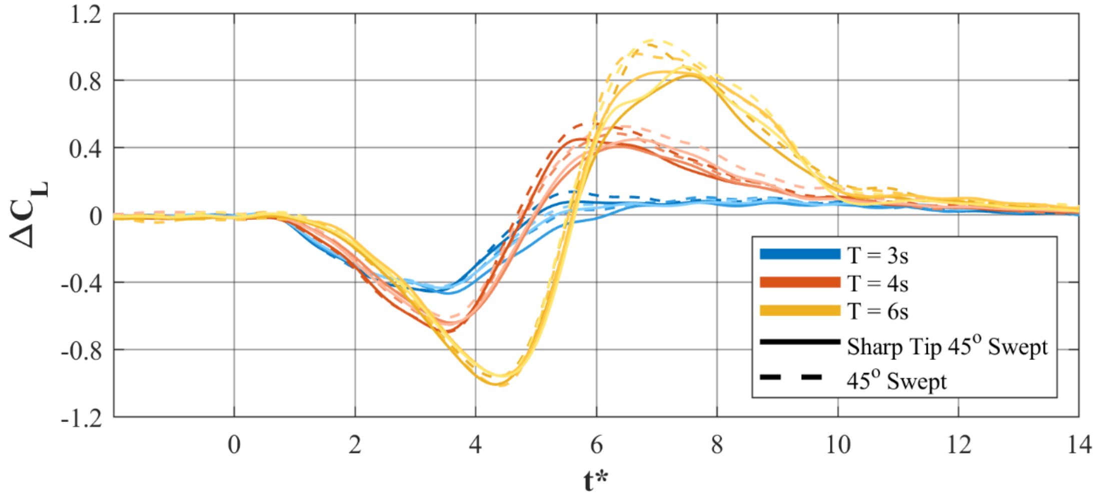

Figure 4.15 : Tip geometry effect on ΔC_L for the case of $h/c = -0.75$, for 45° swept wing.

This finding is supported by the flow visualizations shown in Figure 4.16 and Figure 4.17, where the gust–wing interaction is examined through vorticity plots for the base case (*T* = *4s*, *Δy* = *–36mm*). These instants represent the minimum lift condition and the post-minimum phase where the lift starts to rise again and the flow exhibits strong three-dimensional characteristics.

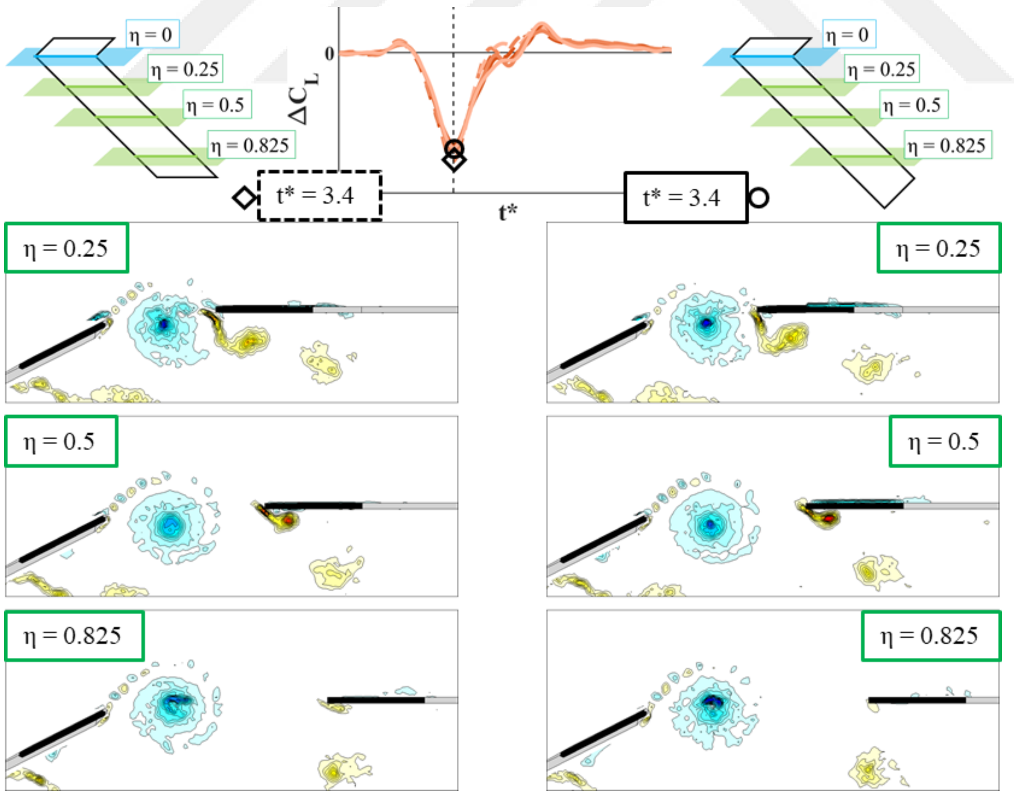

Figure 4.16 : Tip geometry effect on flow structure for the case of *T* = *4s* with *h/c* = *0*, for 45° swept wing, at *t** = *3.4*.

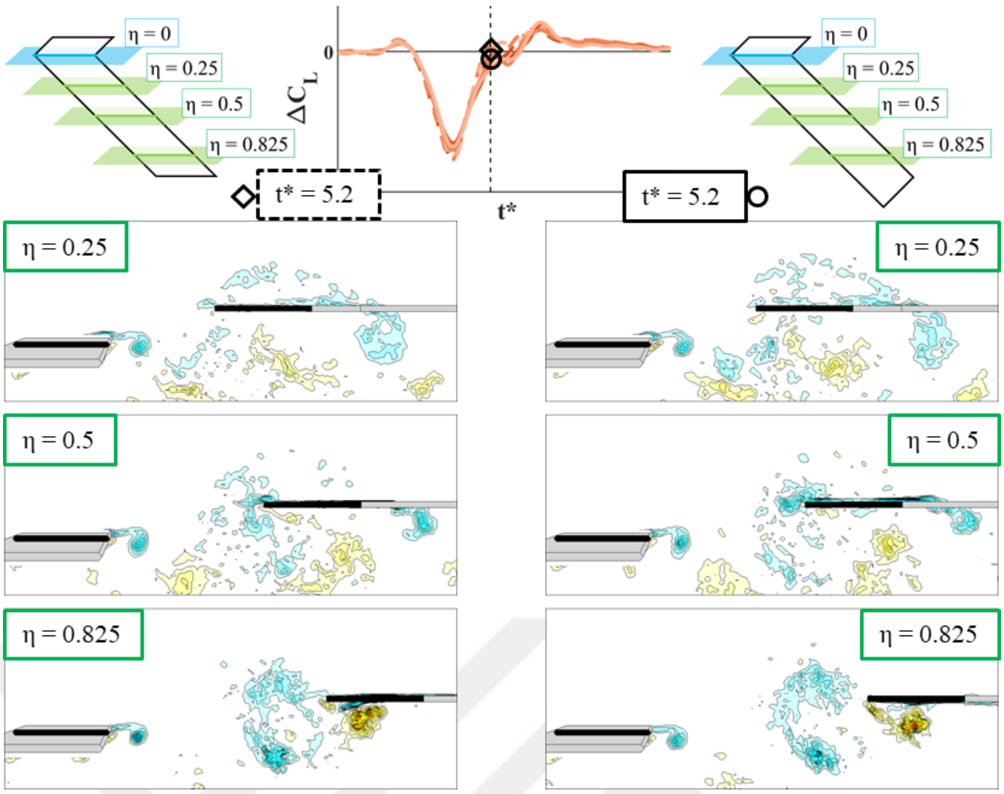

Figure 4.17 : Tip geometry effect on flow structure for the case of $T = 4s$ with $h/c = 0$, for 45° swept wing, at $t^* = 5.2$.

At both instants, the flow topology remains virtually unchanged between the two tip configurations. This demonstrates that the tip geometry, under the current experimental setup and at 0° angle of attack, does not exert a measurable effect on the unsteady lift response or the flow field development.

As in the previous section, this conclusion is also valid for all other test cases and wing configurations. Since the results are qualitatively and quantitatively consistent across the board, only the base case results ($T = 4s$, $\Delta y = -36mm$) are presented here for the sake of brevity.

4.3 Spanwise Superposition of the Time-Shifted 2D Sections

As discussed earlier in this chapter, a notable observation emerged from the instantaneous flow fields of the 45° swept wing configuration: vortex structures that form near the root section are progressively reproduced with a temporal delay as one moves toward the wingtip. This spanwise phase shift suggests that, although the aerodynamic response becomes increasingly three-dimensional, the fundamental flow pattern remains qualitatively similar and 2D across sections when viewed at appropriately shifted instants in time.

Motivated by this observation, the current section explores a simplified modeling approach to reconstruct the lift response of the swept wing by leveraging the quasi-2D nature of the vortex interaction. Specifically, the goal is to determine whether it is possible to predict the lift coefficient curve of the 45° swept wing based solely on the experimental data obtained from the no-swept (rectangular) wing, under the assumption that each spanwise section behaves like a 2D airfoil but with a shifted timeline.

To implement this idea, the rectangular wing, which has the same span as the swept wing, is divided into *N* equal sections along the span. Each of these sections is assumed to experience the same time-dependent lift response, given by the experimentally obtained curve from the no-swept wing. Then, to replicate the swept geometry, each section is geometrically offset in the streamwise direction, forming an equivalent of the 45° swept wing configuration. Figure 4.18 illustrates this process conceptually. The geometric configuration of spanwise sections is shown along with their streamwise offsets.

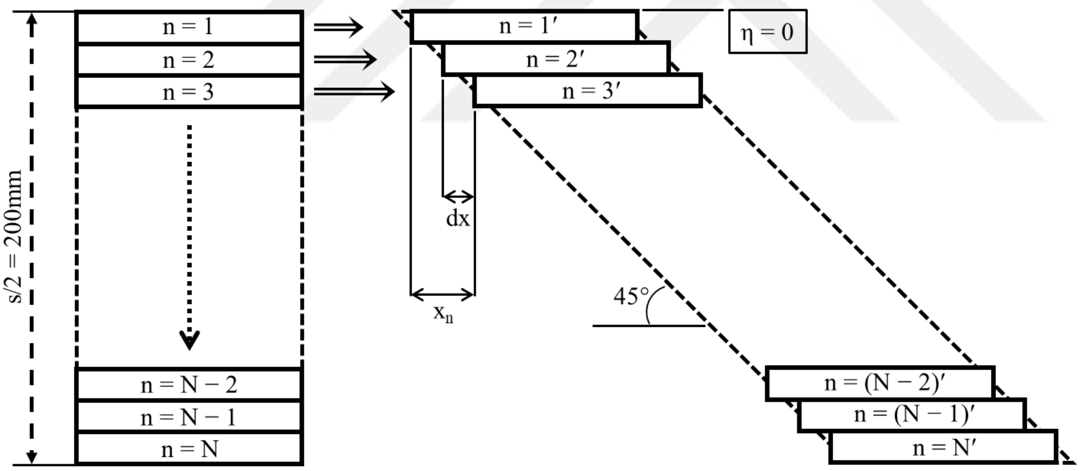

Figure 4.18 : Geometrical offsetting of the divided sections of no-swept wing.

As a result, each section's contribution to the total lift must be shifted in time by an amount determined by its streamwise displacement relative to the root section.

Let *dx* denote the streamwise offset between adjacent spanwise sections and the streamwise displacement of section *n* relative to the root is denoted by $x_n = (n-1)\cdot dx$. Assuming that the negative vortex generated by the gust generator propagates with a speed of V_p, the temporal offset Δt_n for each section is calculated as:

$$\Delta t_n = \frac{x_n}{V_p} \tag{4.3}$$

To formulate the reconstruction method described above, let us define the total approximated total lift response $\Delta C_{L,approx}(t^*)$ of the swept wing as the superposition of time-shifted sectional responses derived from the no-sweep configuration.

We assume that the lift response for each spanwise section ($\Delta C_{L,n}$) is equal to 1/N times the experimentally obtained lift response of the no-swept wing, but time-shifted based on the streamwise offset of that section as,

$$\Delta C_{L,n}[t^*] = \frac{\Delta C_L[t^* - \Delta t_n]}{N} \tag{4.4}$$

and the time-shifted lift responses are superimposed to construct the approximated total lift response of the swept wing as shown below:

$$\Delta C_{L,approx}(t^*) = \sum_{n=1}^{N} \Delta C_{L,n}[t^*] \tag{4.5}$$

This equation represents the fundamental assumption of the reconstruction methodology, which is the swept wing's transient aerodynamic response can be approximated as the sum of delayed 2D responses, where the delays are solely determined by the geometric projection of the sweep and the propagation speed of the vortex gust.

Before proceeding with the reconstruction, an initial investigation was conducted to assess the sensitivity of the method to the number of sections *N* used in the discretization of the wing span. It was found that increasing or decreasing the number of spanwise segments does not significantly affect the resulting approximated lift response, provided that the number is sufficiently large to capture the gradual sweep-induced delay. Based on this observation, a total of $N = 100$ spanwise sections are selected for the current implementation.

To apply the time-shift operation for each section, an estimate for the propagation speed (V_p) of the vortex gust must be determined. In previous studies [25], this speed has been experimentally evaluated under various configurations (Table 4.2). For the case of $T = 4s$ and in the absence of the wing downstream, the propagation speed of the generated negative vortex is measured to be approximately *52.14 mm/s*, while the freestream velocity is equal to *100 mm/s.*

Table 4.2 : Vortex gust characterization results (adopted from Tilki) [25].

	V_{max} (m/s)	GR	r @ $V_{max\_downs.}$ (mm)	We	V_p (mm/s)	V_p/U_∞
NoWing T03	-0.12	1.2	20	0.4	58.9	0.59
NoWing T04	-0.13	1.3	21.4	0.428	52.14	0.52
NoWing T06	-0.105	1.05	20	0.4	47.63	0.48
FP-36mm T03	-0.16	1.6	21.8	0.436	38.1	0.38
FP-36mm T04	-0.145	1.45	24.2	0.484	36	0.36
FP-36mm T06	-0.19	1.9	32	0.64	36	0.36
FP-111mm T03	-0.16	1.6	23.1	0.462	61.2	0.61
FP-111mm T04	-0.13	1.3	22.8	0.456	58.8	0.59
FP-111mm T06	-0.15	1.5	33.6	0.672	43.1	0.43

In contrast, when a no-swept wing is placed in the downstream position, replicating the base case configuration with $T = 4s$ and $\Delta y = -36mm$, the propagation speed of the same vortex structure drops to *36 mm/s*. This reduction in propagation speed is attributed to the direct interaction between the vortex and the wing in the $\Delta y = -36mm$ case. Here, the vortex trajectory intersects the wing's leading edge, causing a form of vortex encounter that slows the downstream progression of the gust.

For the $T = 4s$ *with* $\Delta y = -111mm$ case, the vortex trajectory ($h/c = -0.75$) remains entirely below the pressure side of the wing, meaning there is no direct interaction with the wing surface. In this case, the presence of the wing leads to an increase in the propagation speed compared to that of the absence of the wing. As seen in Table 4.2, the measured value of V_p is *58.8 mm/s*, which is higher than the *52.14 mm/s* obtained in the absence of the downstream wing. This behavior is linked to the passage of the vortex below the wing, possibly assisted by the flow deflection and suction effect around the lower surface (pressure side).

The time-shifting strategy is applied to both test cases ($\Delta y = -36mm$ and $\Delta y = -111mm$ *for* $T = 4s$). Two different V_p values are used for each configuration, which are the one measured in the presence of the wing and in the absence of the wing, to evaluate the sensitivity of the results to this parameter. The shifted responses from all sections are then superimposed to construct an estimated lift response for a 45° swept wing.

The results of this estimation is shown in Figure 4.19 for the case of $T = 4s$ *and* $\Delta y = -36mm$. The red curves shows the experimental response of the wings. The orange and the blue curves corresponds to the predicted lift responses using the propagation speed in the presence of the wing downstream (*36 mm/s*), and the propagation speed in the absence of the wing downstream (*52.14 mm/s*). Both estimates attempt to reconstruct the swept-wing behavior solely from the known response of a no-swept configuration.

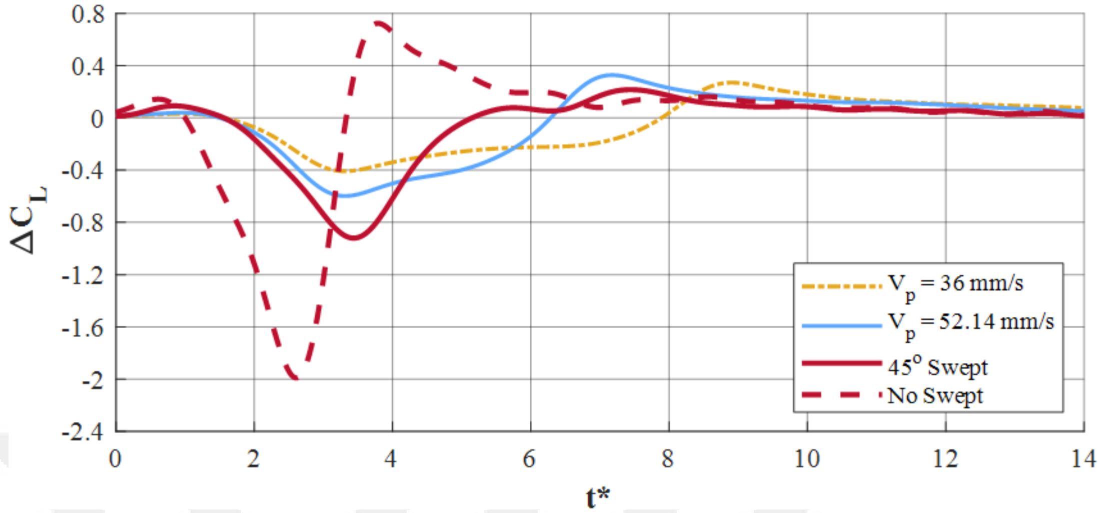

Figure 4.19 : Time-shifted lift transient for the case of $T = 4s$ with $\Delta y = -36mm$, by using propagation speeds with presence and absence of the wing.

Similarly, Figure 4.20 presents the results for the $T = 4s$ and $\Delta y = -111\ mm$ case. As before, the red lines show the experimental data. The blue and green dashed lines depict the predicted lift responses based on propagation speeds of *52.14 mm/s* (in the absence of the wing) and *58.8 mm/s* (in the presence of the wing). These comparisons offer insights into how well the spanwise temporal shift mechanism captures the physics of sweep-induced delay, especially under conditions where the vortex gust follows different trajectories relative to the wing.

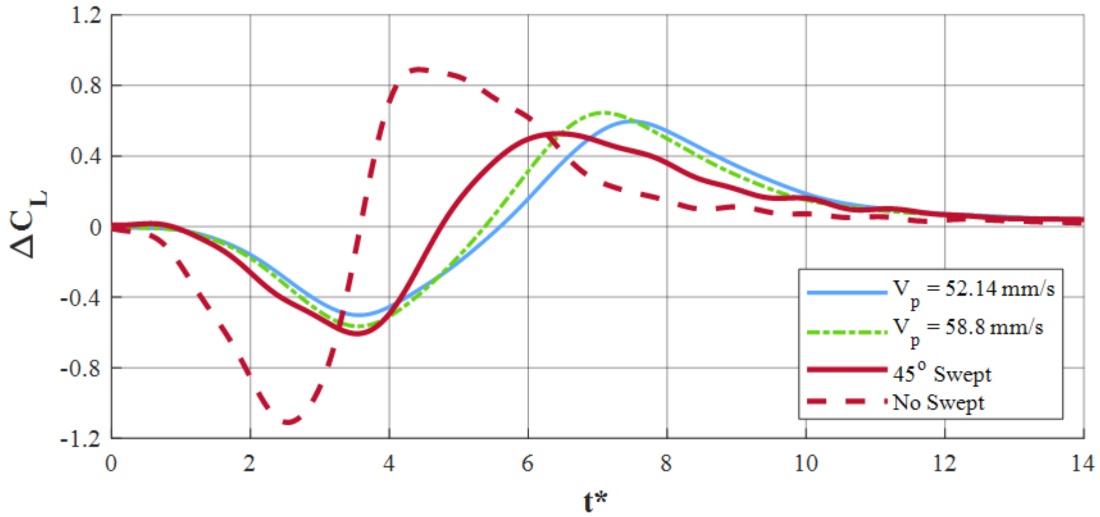

Figure 4.20 : Time-shifted lift transient for the case of $T = 4s$ with $\Delta y = -111mm$, by using propagation speeds with presence and absence of the wing.

As can be seen from the Figure 4.20, for the *Δy = –111mm* case, applying the experimentally measured propagation speed in the presence of the wing yields a time-shifted lift response that aligns very well with the experimental data of the 45° swept wing. This agreement confirms the validity of the time-shifting approach when an appropriate propagation speed is used.

However, for the *Δy = –36mm* scenario, it becomes evident that a more suitable (higher) value of propagation speed must be selected. It is reasonable to expect that introducing a swept wing may lead to an increase in the propagation speed. This hypothesis is motivated by the observation from the *Δy = –111mm* case, where the presence of a wing, with the vortex passing underneath through the pressure side, is found to accelerate the downstream motion of the vortex. A similar mechanism may be at play in the *Δy = –36mm* case, where the swept geometry of the 45° swept wing could promote a comparable suction effect, thus increasing the vortex propagation speed relative to the no-wing scenario.

To test this assumption, a new estimation of the propagation speed is introduced. In the case without a wing, the propagation speed was *52.14 mm/s*, while the addition of a no-swept wing caused it to drop to *36 mm/s* (a decrease of *16.14 mm/s*). By symmetry of reasoning, it is hypothesized that adding a 45° swept wing could instead increase the speed by a similar amount. Accordingly, the propagation speed is set to *68.28 mm/s* in the time-shifting method. Using this updated value, the time-shifting procedure is re-applied, and the resulting lift response is shown in Figure 4.21.

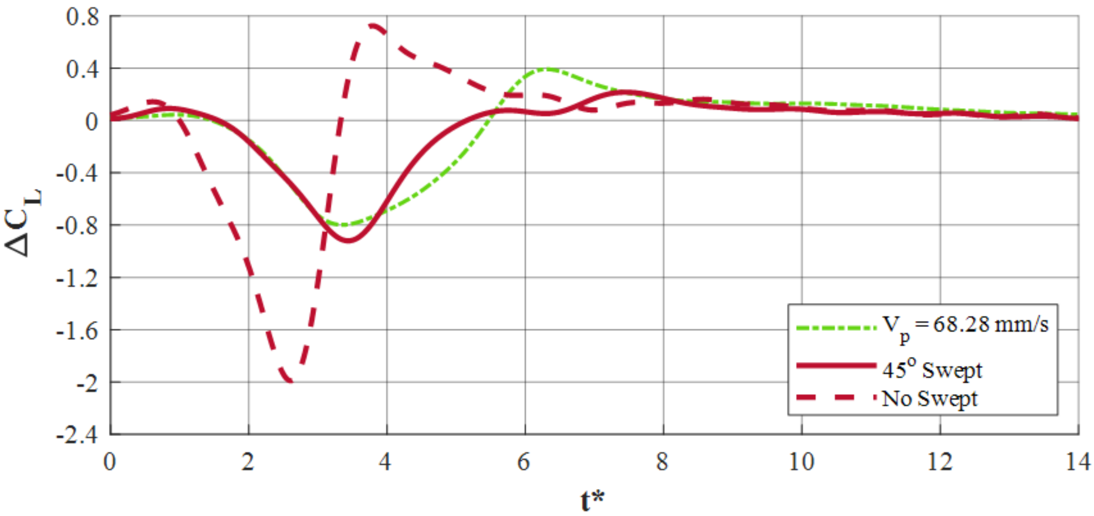

Figure 4.21 : Time-shifted lift transient for the case of *T = 4s* with *Δy = –36mm*, by using an increased propagation speed.

In this figure, the new predicted lift response (green dashed line) shows a strong agreement with the experimentally measured lift transient of the 45° swept wing, reinforcing the interpretation that the swept geometry facilitates faster vortex progression across the span. This outcome further supports the idea that sweep not only induces a temporal phase shift in lift response but may also influence the gust's propagation speed due to geometric and aerodynamic effects such as suction or flow channeling beneath the wing.

5. CONCLUSION

In this study, discrete vortex gust encounter experiments are conducted in a free-surface water channel on several wing configurations, including a no-swept flat plate wing and two swept wing models with differing tip geometries: a sharp tip and a tip aligned with the freestream. Additionally, two submergence levels to address the symmetry plane issue are tested for the swept wing models to examine their effect on gust response. The findings from these experiments can be summarized as follows:

- Comparison between standard submergence level, where the water level coincides with the wing's symmetry axis (root section), and a deeper submergence including 15% of the opposite half-span (creating a partially V-shaped model) revealed no significant influence on the aerodynamic response. This is observed at zero angle of attack, both in terms of lift transient behavior and instantaneous flow structures.

- The two swept wing models, one with a sharp tip and the other with a tip section aligned with the freestream, also demonstrated negligible differences in aerodynamic response. Again, both lift transient data and flow field visualization support this conclusion, particularly at zero angle of attack.

- The sweep angle introduced a notable time delay in the lift response to vortex gust encounters and a reduction of lift amplitude compared to the no-swept configuration.

- The wing sweep had minimal effect on the integrity of the 2D vortex core. The gust maintained its two-dimensional characteristics until directly encountering the corresponding leading edge, particularly near root regions.

- The time shift in lift response observed along the wing span indicates that different sections of the swept wing experienced the gust at slightly different times. This phase lag was confirmed by comparing instantaneous flow visualizations along the span.

- By applying a time shift to the no-swept wing's lift response, based on the propagation speed of the vortex, a good approximation of the 45° swept wing's transient lift profile is obtained. This insight may prove valuable for future gust mitigation strategies in aircraft design.

These findings collectively underscore the aerodynamic response of finite wings under discrete vortex gust encounters and highlight the role of sweep geometry in shaping unsteady lift dynamics. While the variations in submergence level and tip geometry showed minimal impact under the specific test conditions, the influence of sweep angle emerged as a critical factor in both delaying and attenuating lift responses. These observations support the value of simplified modeling techniques, such as time-shifted lift profiles, to approximate complex gust interactions on swept configurations. The work contributes a foundational understanding that may be extended and refined through future experimentation.

Future studies could expand the investigation to include non-zero angles of attack, which are expected to introduce additional flow complexity and potentially alter the role of sweep and tip geometry in gust response. Similarly, evaluating gust encounters across a broader range of sweep angles would enhance understanding of the interplay between sweep-induced flow structures and gust dynamics. Another promising avenue involves further exploring the applicability of the time-shift method: while it proved effective under zero angle of attack conditions, its robustness under varying angles of attack and different gust typologies remains an open question. Extending these methodologies could ultimately inform more resilient wing designs and gust mitigation strategies in real-world flight environments.

REFERENCES

[1] Jones, A. R., Cetiner, O., & Smith, M. J. (2022). Physics and Modeling of Large Flow Disturbances: Discrete Gust Encounters for Modern Air Vehicles. *Annual Review of Fluid Mechanics*, *54*(Volume 54, 2022), 469–493. https://doi.org/https://doi.org/10.1146/annurev-fluid-031621-085520

[2] Gloutak, D., Jansen, K. E., & Farnsworth, J. A. (2023). Aerodynamic Performance of Swept Wings in Unsteady Streamwise Flow. In *AIAA SCITECH 2023 Forum*. American Institute of Aeronautics and Astronautics. https://doi.org/doi:10.2514/6.2023-1231

[3] Wild, O., Gementzopoulos, A., & Jones, A. (2024). Navigating unsteady airwakes: Three-dimensionality and sideslip in strong transverse gust encounters. In *AIAA SCITECH 2024 Forum*. American Institute of Aeronautics and Astronautics. https://doi.org/doi:10.2514/6.2024-1120

[4] Wagner, H. (1925). *Über die Entstehung des dynamischen Auftriebes von Tragflügeln*. VDI-Verl. http://eudml.org/doc/204029

[5] Küssner, H. G. (1936). Zusammenfassender Bericht über den instationären Auftrieb von Flügeln. *Luftfahrtforschung*, *13*, 410–424.

[6] von Kármán, T. H., & Sears, W. R. (1938). Airfoil Theory for Non-Uniform Motion. *Journal of the Aeronautical Sciences*, *5*(10), 379–390. https://doi.org/10.2514/8.674

[7] Adamczyk, J. J. (1974). Passage of a Swept Airfoil through an Oblique Gust. *Journal of Aircraft*, *11*(5), 281–287. https://doi.org/10.2514/3.59240

[8] Perrotta, G., & Jones, A. R. (2017). Unsteady forcing on a flat-plate wing in large transverse gusts. *Experiments in Fluids*, *58*(8), 101. https://doi.org/10.1007/s00348-017-2385-z

[9] Corkery, S. J., Babinsky, H., & Harvey, J. K. (2018). On the development and early observations from a towing tank-based transverse wing–gust encounter test rig. *Experiments in Fluids*, *59*(9), 135. https://doi.org/10.1007/s00348-018-2586-0

[10] Biler, H., Sedky, G., Jones, A. R., Saritas, M., & Cetiner, O. (2020). Experimental Investigation of Transverse and Vortex Gust Encounters at Low Reynolds Numbers. *AIAA Journal*, *59*(3), 786–799. https://doi.org/10.2514/1.J059658

[11] Sedky, G., Biler, H., & Jones, A. R. (2022). Experimental Comparison of a Sinusoidal and Trapezoidal Transverse Gust. *AIAA Journal*, *60*(5), 3347–3351. https://doi.org/10.2514/1.J061365

[12] Gementzopoulos, A., Sedky, G., & Jones, A. (2024). Role of vorticity distribution in the rise and fall of lift during a transverse gust encounter.

Physical Review Fluids, *9*(1), 14701. https://doi.org/10.1103/PhysRevFluids.9.014701

[13] Badrya, C., Jones, A. R., & Baeder, J. D. (2021). Unsteady Aerodynamic Response of a Flat Plate Encountering Large-Amplitude Sharp-Edged Gust. *AIAA Journal*, *60*(3), 1549–1564. https://doi.org/10.2514/1.J060683

[14] Biler, H., Badrya, C., & Jones, A. R. (2019). Experimental and Computational Investigation of Transverse Gust Encounters. *AIAA Journal*, *57*(11), 4608–4622. https://doi.org/10.2514/1.J057646

[15] Cem Gözükara, A., Elif, A., Soy, K., & Cetiner, O. (2022). DÜZ PLAKA ŞEKLİNDEKİ BİR KANAT ÜZERİNDE GİRDAP TİPİ TEKİL SAĞANAK ETKİLERİNİN DENEY KARŞILAŞTIRMALI HESAPLAMALI İNCELEMESİ. In *UHUK-2022-051, 9. Ulusal Havacılık ve Uzay Konferansı*.

[16] Soy, K., Tugan, E., Acar, E., & Cetiner, O. (2023). Experimental Investigation of Discrete to Continuous Vortex Gust Encounters. In *AIAA SCITECH 2023 Forum*. American Institute of Aeronautics and Astronautics. https://doi.org/doi:10.2514/6.2023-1621

[17] Qian, Y., Wang, Z., & Gursul, I. (2022). Interaction of quasi-two-dimensional vortical gusts with airfoils, unswept and swept wings. *Experiments in Fluids*, *63*(8), 124. https://doi.org/10.1007/s00348-022-03477-8

[18] Riddle, T. W., Rogers, S. E., Ross, J. C., & Cummings, R. M. (1998). A numerical analysis of three-dimensional vortex trapping. *Aircraft Design*, *1*(1), 61–73. https://doi.org/https://doi.org/10.1016/S1369-8869(98)00008-1

[19] Zhu, Y., & Breuer, K. (2023). Flow-induced oscillations of pitching swept wings: stability boundary, vortex dynamics and force partitioning. *Journal of Fluid Mechanics*, *977*, A1. https://doi.org/DOI: 10.1017/jfm.2023.925

[20] Vadher, P., & Babinsky, H. (2024). Experimental Generation of Varied Strength Vortex Gusts. In *AIAA SCITECH 2024 Forum*. American Institute of Aeronautics and Astronautics. https://doi.org/doi:10.2514/6.2024-1121

[21] Ito, Y., Yamamoto, K., Kusunose, K., Koike, S., Nakakita, K., Murayama, M., & Tanaka, K. (2016). Effect of Vortex Generators on Transonic Swept Wings. *Journal of Aircraft*, *53*, 1–15. https://doi.org/10.2514/1.C033737

[22] Wild, O. D., & Jones, A. R. (2023). Vortex Identification and Quantification on Blunt Trailing-Edge Rotor Blades in Reverse Flow. *AIAA Journal*, *61*(7), 2982–2997. https://doi.org/10.2514/1.J062576

[23] Yilmaz, T. O., & Rockwell, D. (2009). Flow structure on a three-dimensional wing subjected to small amplitude perturbations. *Experiments in Fluids*, *47*(4), 579–597. https://doi.org/10.1007/s00348-009-0637-2

[24] Son, O., & Cetiner, O. (2018). Force-motion phase relations and aerodynamic performance of a plunging plate. *Experiments in Fluids*, *59*(2), 28. https://doi.org/10.1007/s00348-017-2484-x

[25] Tilki, B. (2025). *Characterization of discrete vortex gusts* [Master’s thesis, Istanbul Technical University].

CURRICULUM VITAE

Name Surname : Ozan İbrahimağaoğlu

EDUCATION :

- **B.Sc. :** 2021, Istanbul Technical University, Faculty of Aeronautics and Astronautics, Department of Aeronautical Engineering

PROFESSIONAL EXPERIENCE AND REWARDS:

- 2024–Present: Research Assistant, Faculty of Aeronautics and Astronautics, Aeronautical Engineering Department, Istanbul Technical University

PUBLICATIONS, PRESENTATIONS AND PATENTS:

- Gozukara, A. C.**, Ibrahimagaoglu, O.,** Hizalan, O., & Cetiner, O. (2025). Vortex Gusts Encountered by a Flat Plate at 45° Wing Sweep. *15th International Conference on Computational Heat & Mass Transfer*, May 19-23.
- **Ibrahimagaoglu, O.**, & Cetiner, O. (2025). Experimental Study on Vortex Gust Encountered by a Flat Plate at 45˚ Wing Sweep. *4th International Graduate Research Symposium*, May 12-14.